J. Mech. Phys. Solids 153 (2021) 104456

Contents lists available at ScienceDirect

Journal of the Mechanics and Physics of Solids

journal homepage: www.elsevier.com/locate/jmps

Mechanical behavior of photopolymerized materials

Roberto Brighenti *, Mattia Pancrazio Cosma

Department of Engineering and Architecture, University of Parma, Parco Area delle Scienze 181/A, 43124 Parma, Italy

ARTICLE INFO

Keywords:
Polymers
Photopolymerization
Chain density
Mechanical response
Optimal polymer microstructure

ABSTRACT

The photopolymerization process used for the production of additively manufactured polymers employed in advanced applications, enables obtaining objects spanning a large dimensional scale thanks to the molecular size achievable by the solidification process. In fact, the photopolymerization is based on the physical-chemical network cross-linking mechanism taking place at the nanoscale. Since the starting raw material is a liquid resin that progressively becomes solid upon the irradiation by a suitable light source, the mechanical properties – and so the corresponding mechanical response of the final printed structural material – heavily depend on the degree and distribution of the polymerization induced in the material itself. In the present study, starting from the governing equations of the light-induced polymerization process, we determine the chain density formed within the solid domain. Then, the mechanical response of photopolymerized elements obtained with different photopolymerization parameters is investigated. Moreover, the microstructure optimization of polymeric elements in relation to the achievement of the desired mechanical response with the least energy spent in the polymer's formation, is studied. Finally, some interesting considerations related to the modeling of the photopolymerization process are outlined.

1. Introduction

The use of light to induce a controlled polymerization has been recognized to be an efficient and powerful strategy to synthesize polymers suitable for the production of advanced materials. In fact, a solid polymer can be obtained by inducing the solidification of a liquid resin by harnessing the light-activation capability of embedded cromophores (photoinitiators) exposed to a suitable light source, whose electromagnetic spectrum for the polymerization to occur often falls within the ultraviolet or the visible region. Structural changes in the material takes place at the nanoscale level because of the cross-linking occurring between chains when exposed to light, a process usually referred to as curing (Phillips, 1984; Chen et al., 2016; Yamaguchi and Nakamoto, 1998; Bowman and Kloxin, 2008). The most advanced free radical initiation technologies used in the photo-induced polymerization, allow using a wide range of monomers and photoinitiators capable of reacting in the presence of radicals, such as (meth) acrylate monomers and (meth) acrylated oligomers (Andrzejewska and Grajek, 2017).

Polymeric materials obtained through light-induced polymerization are nowadays mainly produced through additive manufacturing (AM) processes, such as in the so-called stereolithography technology, and find extensive use in medicine, nanotechnology, development of small scale metamaterials, fabrication of materials used in advanced technological applications (optoelectronics, holographic data storage, …), energy, photoresisting materials, etc. (Andrzejewska and Grajek, 2017; Bella and

* Corresponding author.
E-mail address: roberto.brighenti@unipr.it (R. Brighenti).

https://doi.org/10.1016/j.jmps.2021.104456
Received 17 November 2020; Received in revised form 5 February 2021; Accepted 16 April 2021
Available online 28 April 2021

Nomenclature

A	Attenuation coefficient or material's absorbance
$\boldsymbol{A}$	Depletion matrix of the FE discretized domain
A_{abs}, A_{pol}, A_{mon}	Absorption due to photoabsorbers, due to monomer converted into polymer and due to un-polymerized monomers, respectively
b	Length of Kuhn's segments
c_a	Concentration of polymer's active chains
C_I	Concentration of photo-initiator molecules (Ph_I)
C_M	Concentration of monomer molecules (M)
C_R	Concentration of free radicals ($R^\bullet$)
$\boldsymbol{D}$	Stabilization matrix of the numerical solution of the light diffusion problem
$\boldsymbol{E}$	Light gradient matrix of the domain discretized with FEs
$\boldsymbol{f}$	Force in a single polymer chain
$\boldsymbol{F}$	Deformation gradient tensor
h	Thickness of the photopolymerized layer
I	Laser light intensity
I_m	Maximum laser light intensity on the irradiated surface
$J = \det\boldsymbol{F}$	Relative volume change of the material
k_B	Boltzmann's constant
k_d, k_p, k_t	Reaction rate constants of the photopolymerization reactions
k_{pr}	Photodecomposition rate
$\boldsymbol{l}(\boldsymbol{X}, t)$	Unit vector identifying the incoming light beam direction
$\boldsymbol{L}$	Velocity tensor gradient of deformation
N	Number of Kuhn's segments in a polymer chain
$\boldsymbol{n}$	Unit vector normal to the free surface of the domain hit by the light beam
m	Number of radicals generated in the photodecomposition
$\boldsymbol{P}$	First Piola stress tensor
$P^\bullet$	Functional groups (growing polymer chains)
P_{dead}	Dead polymer chains (chains that completed the growth process)
$\boldsymbol{Q}$	Vector of the nodal values of the incoming light intensity
$R^\bullet$	Free radicals
t	Time
τ_r, $\overline{\tau}_r$	Viscous relaxation time of a generic polymer and of a fully cured one, respectively
t_c	Curing time
T	Temperature
v	Linear velocity of the light beam
w	Width of the photopolymerized layer
$f(\boldsymbol{r})$, $f_0(\boldsymbol{r})$	Dimensionless distribution function of the chains' end-to-end vector and the corresponding one at the initial stress-free state, respectively
μ, $\overline{\mu}$	Shear modulus of the photopolimerized polymer and that of the fully-cured material, respectively
ψ	Deformation energy in a single polymer chain
Ψ	Deformation energy per unit volume of polymer
$\varphi(\boldsymbol{r})$	Distribution function of the chains' end-to-end vector
ϱ	Degree of cure (or degree of conversion, DoC) achieved during the photopolymerization
$\boldsymbol{\sigma}$	Cauchy stress tensor
θ	Photo-initiator molar absorptivity
$[\blacksquare]$	Concentration of the chemical species represented by ■
$\widetilde{\blacksquare}$	Average value of the generic quantity ■

Bongiovanni, 2013; Buss and Miyake, 2018). Thanks to the possibility of controlling in space and time the polymerization process, the potentiality to produce new materials is readily achievable, and high-precision small scale objects, not allowed by other productions technologies, can now be easily obtained (Bikas et al., 2016; Brighenti et al., 2020).

Typically, the curing process is obtained by using UV radiation, although the development of technologies based on the visible light – characterized by important advantages in terms of simplicity and safety – are now available. It is worth recalling that the polymerization process can be also triggered by using only thermal energy, even if photo-driven polymerization typically has superior characters, such as the high polymerization rates achievable and the greater environmental safety because the use of volatile organic solvents can be avoided.

During free radical photopolymerization the monomer solidification is obtained upon irradiation of the monomer liquid, doped

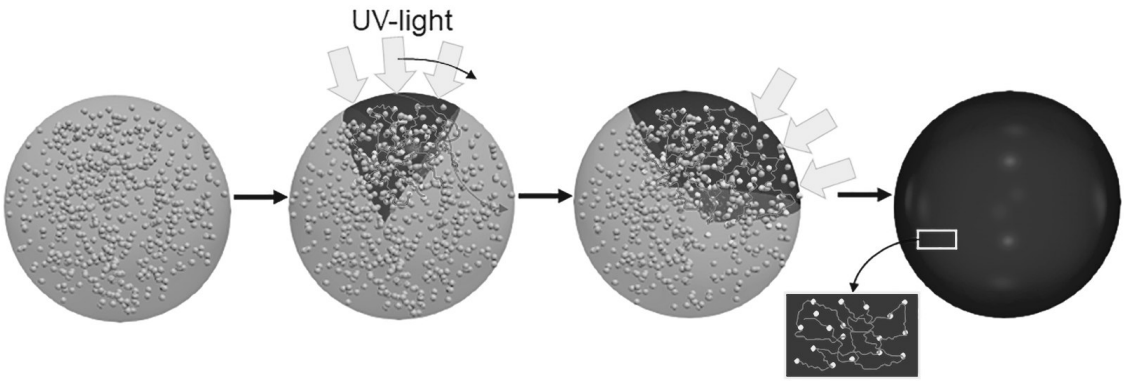

Fig. 1. (Color online) Scheme of the photopolymerization process: from the liquid resin (left) to the final solid cross-linked network (right).

with a small amount of so-called photoinitiator molecules, with a selective light leading to a highly cross-linked polymer network. The photoinitiators are compounds that, exposed to light, decompose into reactive species, enabling the activation of the polymerization process induced by specific functional groups.

Structural and chemical properties of the final material can be tuned up thanks to polymer subunits (chromophores) internally embedded in the raw material, or by addition of external photosensitive molecules. Usually, a photopolymer is made of a mixture of multifunctional monomers and oligomers whose proportions are defined in order to achieve the desired final physical properties. Photopolymers are involved in the curing process, in which oligomers are cross-linked upon exposure to light, leading to a highly entangled network polymer, typically belonging to the thermoset family (Long et al., 2013; Sain et al., 2018, 2009).

In the present paper, we investigate the mechanical properties of polymeric materials obtained through photopolymerization; according to the light-induced solidification process dependent on the way the light is spread onto the initial liquid monomer domain, the spatial cross-linked chain density arrangement arising in the underneath network is determined.

Within the context of mechanical modeling of polymeric materials, several methods have been proposed (Gartner and Jayaraman, 2019), ranging from continuum models (Fleer and Skvortsov, 2012), molecular approaches (Jha and Tsige, 2013), multiscale methods (Talebi et al., 2014; Valavala et al., 2007), to those assuming a predefined chains arrangement within the network (such as the eight-chain model, Arruda and Boyce, 1993; Dupaix and Boyce, 2007). We adopt a statistical description of the polymer chain arrangement linking the microscale network features to the mechanical response at the mesoscale level; this approach is particularly suitable for determining the macroscopic mechanical properties of a polymer obtained via photopolymerization.

By properly driving the photopolymerization process, the distribution of the mechanical properties can be precisely controlled. This allows optimizing the solidification process in relation to some suitable objective functions, whose minima ensures the achievement of the optimum mechanical response with the least energy spent on the polymer formation. Moreover, we investigate the effects of the peak light intensity and of the translational laser speed on the mechanical behavior of printed structural elements. We demonstrate how different can be the mechanical response of structural elements under the same boundary conditions, by simply printing them with different photopolymerization setups. Furthermore, some interesting insights into the photopolymerization process and its modeling are discussed.

The paper is organized as follows: Sect. 2 illustrates the governing equations involved in the multi-physics processes related to the chemistry (Sect. 2.1) and light diffusion (Sect. 2.2) in materials synthesized through photopolymerization. Sect. 3 is devoted to the micromechanical modeling of polymers by using the above-mentioned statistical-based approach; further, the viscous response, quantified through the characteristic relaxation time, is also addressed with respect to the polymer chain density achieved in the material. Sect. 4 considers the problem of the optimal photopolymerization by introducing some suitable mechanical-related objective functions, while Sect. 5 provides some insight into the computational implementation of the outlined multiphysics problem. Finally, Sect. 6 illustrates some numerical examples and Sect. 7 presents some closing remarks and future perspectives.

2. Governing equations of the chemical-physics problem

2.1. Equations governing the chemistry of photopolymerization

Photopolymerization, whose reactions are described by a set of reaction equations accounting for the penetration of light coming from the laser source into the solution, is a chemical-physics process that typically uses UV light to induce the free radical polymerization of an initially liquid monomer. At the beginning, the liquid monomer M (whose molecule concentration is $C_M(\boldsymbol{X},t)$, being $\boldsymbol{X},t$ the position vector in the reference configuration in the 3D space and the time, respectively) is irradiated by the UV light. For sake of simplicity hereafter we assume that during the photopolymerization the configuration of the domain does not change, i.e. we neglect any effect due to geometrical distortions; beyond that, the study of a single layer of monomer justifies such an assumption being its configuration not influenced by previously solidified surrounding layers. Upon light irradiation, the photo-initiators molecules (Ph_I) present in the liquid monomer with concentration $C_I(\boldsymbol{X},t)$ are converted into free radicals ($R^\bullet$) whose concentration is $C_R(\boldsymbol{X},t)$. Once free radicals appear, they react with the monomer molecules leading to the activation of the functional groups $P^\bullet$ that grow within the

material by reacting with other monomer molecules and so forming polymer chains (Fig. 1).

The growth and propagation of chains is active until a termination stage is reached, i.e. a chain stops growing when it: *i*) meets a free radical ($P^{\bullet} + R^{\bullet} \overset{k_t}{\rightarrow} P_{\text{dead}}$) or *ii*) it binds to another chain hit along its growth path ($P^{\bullet} + P^{\bullet} \overset{k_t}{\rightarrow} P_{dead}$) (Wu et al., 2018; Anastasio et al., 2019).

The scheme of the reactions taking place during the polymerization can be summarized as follows:

$$\begin{array}{lll} 1) & Ph_I \overset{k_{pr}}{\rightarrow} 2R^{\bullet} & \text{Photo} - \text{initiators decomposition} \\ 2) & R^{\bullet} + M \overset{k_p}{\rightarrow} P^{\bullet} & \text{Onset of a polymer chain} \\ 3) & P^{\bullet} + M \overset{k_p}{\rightarrow} P^{\bullet} & \text{Growth of a polymer chain} \\ 4a) & P^{\bullet} + P^{\bullet} \overset{k_t}{\rightarrow} P_{\text{dead}} & \text{Chain growth termination} \\ 4b) & P^{\bullet} + R^{\bullet} \overset{k_t}{\rightarrow} P_{\text{dead}} & \end{array} \tag{1}$$

where k_{pr}, k_p and k_t are the rate constants characterizing the chemical process (Bowman and Kloxin, 2008; Andrzejewska, 2001; Anastasio et al., 2019).

The process described above corresponds to a progressive reduction of the monomer concentration, because of the monomer's molecules combination with radicals, leading to the chains formation (cross-linking); correspondingly, the chains density increases and the material progressively solidifies showing an increase of its mechanical stiffness. The quantitative description of the chain formation and growth is usually related to the so-called degree of cure (DoC, degree of conversion), defined as:

$$\varrho(\boldsymbol{X}, t) = 1 - C_M(\boldsymbol{X}, t)\ C_{M0}^{-1}(\boldsymbol{X}) \tag{2}$$

providing the amount of the monomer molecules converted into polymer chains, being $C_{M0}(\boldsymbol{X}) = C_M(\boldsymbol{X}, t = 0)$. At the beginning of the light irradiation process it is $\varrho(\boldsymbol{X}, 0) = 0$, while $\varrho(\boldsymbol{X}, t) \rightarrow 1$ (i.e. $C_M(\boldsymbol{X}, t) \ll C_M(\boldsymbol{X}, t = 0)$) when the chain formation is almost complete, i.e. for a sufficiently high value of the curing time t at a given value of the laser light intensity.

From the above description, it appears that the degree of cure plays a fundamental role in the characterization of photopolymerized materials, since it is readily related to the concentration of active chains $c_a(\boldsymbol{X}, t)$ forming the polymer network (i.e. those fully connected to the neighbouring chains) capable of carrying a mechanical stress (Vernerey et al., 2017).

The relationship existing between the degree of cure and the chain concentration has been provided by (Zarrelli et al., 2010) to be given by the following exponential relationship

$$c_a(\boldsymbol{X}, t) = \frac{1}{3\ k_B T}\left\{E_d + E_c \exp\left[s\left(\varrho(\boldsymbol{X}, t) - \varrho_{gel}\right)\right]\right\} \tag{3}$$

derived by assuming an incompressible behavior of the polymer, where $\mu(\boldsymbol{X}, t)$ is the shear modulus (related to the chain concentration through the well-known relation $\mu(\boldsymbol{X}, t) = c_a(\boldsymbol{X}, t) k_B T$ (de Gennes and Leger, 1982)), k_B, T are the Boltzmann's constant and the absolute temperature, respectively, while E_c, E_d and s are fitting parameters and ϱ_{gel} is the degree of cure at the gelation point, i.e. at $t = t_{gel}$ when the material start becoming stiffer and stiffer as the photopolymerization proceeds.

The pointwise variation of the degree of cure in the material depends on both the light intensity $I(\boldsymbol{X}, t)$ and its time duration at the point of interest. It is worth mentioning that the first models proposed to describe the photopolymerization process, enabling the prediction of the liquid-solid transformation only, were mainly based on energetic approaches (Brighenti et al., 2020; Yamaguchi and Nakamoto, 1998), while the network growth was not considered and so the precise mechanical properties evolution of the material were not achievable.

On the other hand, kinetic models allowing a quantitative description of the photopolymerization process through a set of first order partial differential equations governing the involved chemical reactions, have been recently extended and used to simulate real photopolymerization processes (Anastasio et al., 2019).

The evolution of the chemical species involved in the photopolymerization can be expressed through the following differential equations (Wu et al., 2018):

$$\dot{C}_I(\boldsymbol{X}, t) = -k_{pr}\ I(\boldsymbol{X}, t)\ C_I(\boldsymbol{X}, t) \tag{4a}$$

$$\dot{C}_R(\boldsymbol{X}, t) = -m\ \dot{C}_I(\boldsymbol{X}, t) - m\ k_t(\boldsymbol{X}, t)[C_R(\boldsymbol{X}, t)]^2 \tag{4b}$$

$$\dot{C}_M(\boldsymbol{X}, t) = -k_p(\boldsymbol{X}, t) C_M(\boldsymbol{X}, t) C_R(\boldsymbol{X}, t) \tag{4c}$$

with initial conditions: $C_I(\boldsymbol{X}, t = 0) = C_{I0}$, $C_R(\boldsymbol{X}, t = 0) = C_{R0}$ and $C_M(\boldsymbol{X}, t = 0) = C_{M0}$,. In the above differential equations k_{pr} represents the photodecomposition rate, m is the number of radicals generated in the photodecomposition, k_t is the termination rate (often expressed as $k_t(t) = k_{t0} \cdot p(\varrho)$, where k_{t0} represents the initial termination rate and p is a function depending on the curing evolution), while k_p is the propagation rate which can be also related to the curing evolution. The symbol $\dot{\blacksquare}$ stands for the time derivative of the quantity $\blacksquare$.

By evaluating the time derivative of Eq. (2) and using Eq. (4c), the time rate of the degree of cure can be also expressed as $\dot{\varrho}(\boldsymbol{X}, t) =$

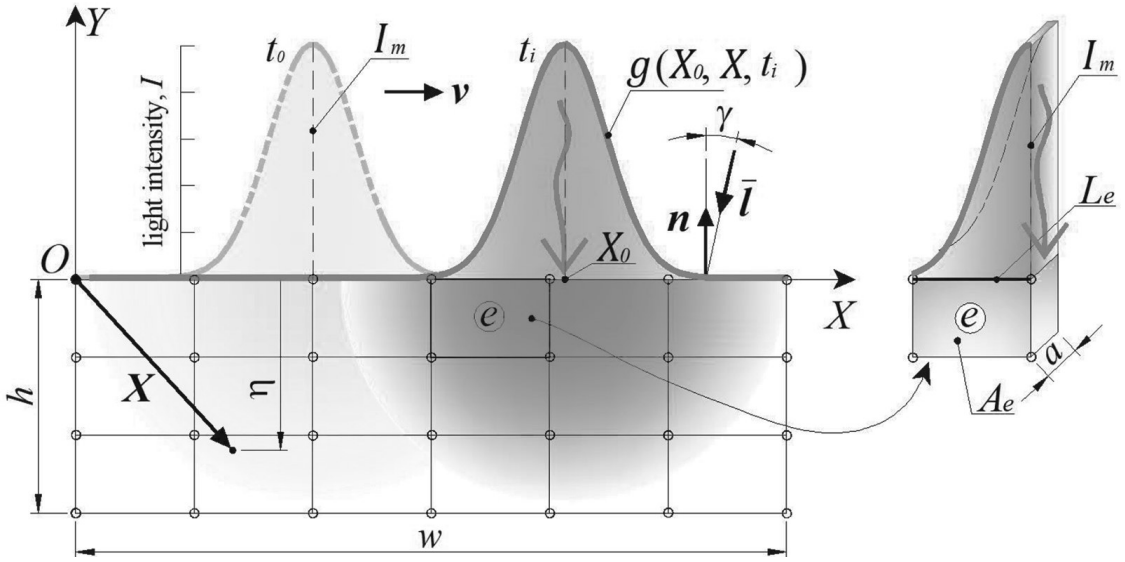

Fig. 2. (Color online) Light coming from a source irradiating from above a rectangular domain $w \times h$; the domain is here represented discretized into finite elements. The light beam is moving from the left to the right hand side at the velocity v. In the numerical solution the nodal values of the light intensity are evaluated through a consistent formulation (see Sect. 5).

$\frac{k_p(\boldsymbol{X},t)\ C_M(\boldsymbol{X},t)\ C_R(\boldsymbol{X},t)}{C_{M0}}$. By assuming $\varrho_{gel} \cong 0$, and indicating with $\overline{\mu}$ the shear modulus of the fully cured material (i.e. that reached for a curing time $t \to \infty$), the chain concentration can be also expressed as :

$$c_a(\boldsymbol{X},t) = \frac{\overline{\mu}}{k_B T} \cdot \exp[\varpi(\varrho(\boldsymbol{X},t) - 1)] \tag{5}$$

while its time derivative becomes $\dot{c}_a(\boldsymbol{X},t) = \varpi\ c_a(\boldsymbol{X},t)\ \dot{\varrho}(\boldsymbol{X},t)$, where ϖ is a model parameter. Once the chain concentration rate $\dot{c}_a(\boldsymbol{X},t)$ is known, the concentration of cross-linked chains at the final curing time t_c, is given by $c_a(\boldsymbol{X},t_c) = c_a(\boldsymbol{X},t=0) + \int_{t_{gel}}^{t_c} \dot{c}_a(\boldsymbol{X},t)\ dt$, where $c_a(\boldsymbol{X},t=0) \cong c_{a,gel} \cong 0$ is the (usually) negligible value of the chain concentration at $t = t_{gel}$.

2.2. Light diffusion governing equations

The diffusion of light within a semi-transparent material is an instantaneous process described by a set of first order elliptic PDEs; the light intensity is attenuated as it travels through the medium and the degree of attenuation is provided by the absorptivity of the material which is dependent on the concentration of the absorbing species and the molar absorptivity of the material itself.

The light intensity distribution within the medium is obtainable by solving the well-known Beer-Lambert law (Davis and Marshak, 2004) expressed by a differential relation between the spatial light intensity decrease rate and the light attenuation. Let us consider a domain occupied by the material to be photopolymerized in its reference configuration, Ω_0, while the corresponding boundary is denoted by $\partial\Omega_0$. A generic point within Ω_0 is indicated with $\boldsymbol{X}$ and the corresponding one in the current deformed configuration Ω (with boundary $\partial\Omega$) is indicated with $\boldsymbol{x}$. In a general 3D framework, the Beer-Lambert law is expressed by the following first-order linear differential equation equipped with the Dirichlet boundary condition:

$$\begin{aligned} \boldsymbol{l}(\boldsymbol{X},t) \cdot \nabla_{\boldsymbol{X}} I(\boldsymbol{X},t) &= -A(\boldsymbol{X},t) I(\boldsymbol{X},t) \quad \text{for } \boldsymbol{X} \in \Omega_0 \\ I(\boldsymbol{X},t) &= \bar{I}(\boldsymbol{X},t) \quad \text{for } \boldsymbol{X} \in \partial\Omega_0 \end{aligned} \tag{6}$$

where ∇ is the gradient operator, while $\boldsymbol{l}(\boldsymbol{X},t)$ is the unit vector of the incoming beam light, $I(\boldsymbol{X},\ t)$ the light intensity at the position $\boldsymbol{X}$ and time t and $A(\boldsymbol{X},t)$ is the attenuation coefficient measuring the light absorbance of the material crossed by light. The latter parameter quantifies the light attenuation occurring because a fraction of light photons traveling through the material is arrested. It is worth mentioning that the local attenuation coefficient $A(\boldsymbol{X},t)$ can be expressed as the sum of the absorbance coming from different contributions provided by the various species constituting the irradiated material, namely the photo-initiator molar absorptivity (θ), the absorption due to photoabsorbers (A_{abs}), that of the converted polymer (A_{pol}) and of the un-polymerized monomers (A_{mon}). It is usually expressed as (Wu et al., 2018; Shao et al., 2014):

$$A(\boldsymbol{X},t) = \theta\ C_I(\boldsymbol{X},t) + A_{abs}(\boldsymbol{X},t) + A_{pol}\ \varrho(\boldsymbol{X},t) + A_{mon}(1 - \varrho(\boldsymbol{X},t)) \tag{7}$$

where C_I is the photo-initiator concentration. Because of the dependence of $A(\boldsymbol{X},t)$ on the light intensity history occurred at a point through the function ϱ, Eq. (6) is highly nonlinear.

Finally, the boundary condition $I(\boldsymbol{X},\ t) = \bar{I}(\boldsymbol{X},t)$ at $\boldsymbol{X} \in \partial\Omega_0$, provides the light intensity distribution on the external boundary of the domain (Fig. 2); in the following, it is expressed as $\bar{I}(\boldsymbol{X},t) = I_m\ g(\boldsymbol{X}_0,\boldsymbol{X},t)$, where I_m is the maximum intensity of the light and $g(\boldsymbol{X}_0, \boldsymbol{X},t)$ is the distribution function of the dimensionless light intensity on the boundary of the domain identified by $Y = 0$ (Fig. 2).

3. Micromechanics of polymers

3.1. Statistical description of the polymer network

The physical state of the network microstructure of a polymeric material can be conveniently described by adopting a statistical approach. Being the underlying polymer's microstructure amorphous, its behavior has been recognized to be mainly governed by entropic effects, and so the entropic energy function fully describes the mechanical response of this class of materials (Vorov et al., 2008). This approach is appropriate for not too large value of the deformation applied to the network; when the stretch applied to the polymer makes the chains approaching their contour lengths, the enthalpic effect enter into play and assumes the main role, while the entropic energy becomes less important.

The classical rubber elasticity theory (Gordon, 1975; Flory, 1953) assumes that the mechanical energy stored in a chain is governed only by the current distance existing between the two chain's extremities (end-to-end vector distance $\boldsymbol{r}$), identified as the points (cross-links) where the chain is jointed to other neighbouring chains; the nature of such connections can be quite different, ranging from strong covalent bonds in thermoset polymers to weaker physical ionic ones in thermoplastic polymers. However, the nature of the bonds does not play a role in the present model.

The most common geometrical model adopted for a polymer chain assumes it to be made of N rigid segments of equal length b (Kuhn's segments), arranged according to the so-called random-walk theory and connected at its extremities to other chains, while no correlation between the segments' directions is usually assumed to exist (freely-jointed chain model, FJC) (Treloar, 1946; Flory, 1969; Flory and Rehner, 1943; Flory et al., 1976). The polymer's microstructure thus results to be made of an entangled arrangement of chains forming the final network.

The statistical-based approach we adopt is based on the assumption that the elastic energy of the material is mainly entropic, as occurs in a not too much stretched entangled network, i.e. stretched well below the maximum elongation allowed by the FJC model, $\lambda_{max} = \sqrt{N}$ (Treloar, 1946). In other words, the energy density must depend mainly on the chains' configuration, while no deformation is assumed to occur within the chain.

In the following, we use a statistical description of the chain distribution by accounting also for the strain-rate effects responsible for the viscoelastic behavior of the material; the latter mechanism can be conveniently described by assuming the chains to be able to rearrange their reciprocal connections in time, i.e. by harnessing the concept of dynamic network (see Sect. 3.2) (Vernerey et al., 2017), resembling the dissipative sliding mechanisms responsible for the viscous behavior.

According to the FJC model, the physical state of a polymer is provided by the knowledge of the end-to-end vector $\boldsymbol{r}$ of all the chains constituting the network; to this end, we here introduce the so-called distribution function $\varphi(\boldsymbol{r})$ providing the number of chains whose end-to-end vector falls within an infinitesimal 3D region in the chains configuration space, centered at $\boldsymbol{r}$. For sake of simplicity, hereafter the position vector $\boldsymbol{X}$ identifying a generic point in the material will be not explicitly indicated. In the reference (macroscopically stress-free) state, such a function is indicated as

$$\varphi_0(\boldsymbol{r}) = c_{a0} \cdot f_0(\boldsymbol{r}) \tag{8}$$

where c_{a0} is the initial chain concentration value (number of active chains, assumed to be produced by the photopolymerization process, $c_{a0} = c_a(t_c)$) per unit volume and $f_0(\boldsymbol{r})$ is a dimensionless distribution function (often assumed to be the standard Gaussian, with mean value $\boldsymbol{r} = 0$ and standard deviation $b\sqrt{N/3}$; the integral of $f_0(\boldsymbol{r})$ evaluated over the whole chain configuration space must be equal to 1 (Doi, 1996). As mentioned above, c_{a0} accounts only for the active or load bearing chains, i.e. those connected at both ends to neighbouring chains.

Any deformation applied to the network, as well as any network chains re-arrangement mechanism occurring in the polymer, are responsible for changing the above-mentioned distribution function $f(\boldsymbol{r},t)$. For sake of brevity, we introduce the following operator, $\langle\blacksquare\rangle = \int_{\Omega}\blacksquare d\Omega = \int_0^{2\pi}\int_0^{\pi}\left(\int_0^{Nb}\blacksquare\, r^2 dr\right)\sin\theta d\theta d\omega$, expressing the integration of the quantity $\blacksquare$ over the chain configuration space; it follows that $c_a(t) = \langle\varphi(\boldsymbol{r},t)\rangle = c_{a0}\langle f(\boldsymbol{r},t)\rangle$, being c_{a0} the initial chain concentration (it is worth mentioning that such a chain concentration c_{a0} does not change in time in absence of any damage (chains rupture) or self healing (chains gain) as will be assumed in the following), so $c_a = c_{a0}\ \forall t \geq t_c$. At a generic time t, the deformation energy per unit volume Ψ stored in the material is obtainable by adding up the energy stored in the single chains $\psi(\boldsymbol{r})$ (typically expressed as a function of $\boldsymbol{r}$) belonging to such a volume; it can be evaluated via the following integral: $\Psi = c_a\langle f(\boldsymbol{r},t)\psi(\boldsymbol{r})\rangle$. For sake of convenience, if the chain concentration does not change in time, it is more useful to evaluate the potential energy $\Delta\Psi(t)$ with respect to the stress-free state,

$$\begin{aligned} &\Delta\Psi(t) = \Psi - \Psi_0 = c_a < \Delta f(\boldsymbol{r},t)\ \psi(\boldsymbol{r}) > \\ &\quad \text{with} \quad \Delta f(\boldsymbol{r},t) = f(\boldsymbol{r},t) - f_0(\boldsymbol{r},0) \end{aligned} \tag{9}$$

since the energy per unit volume stored in the material is always positive, even in the stress-free configuration, i.e. $\Psi_0 = \Psi(t=0) =$

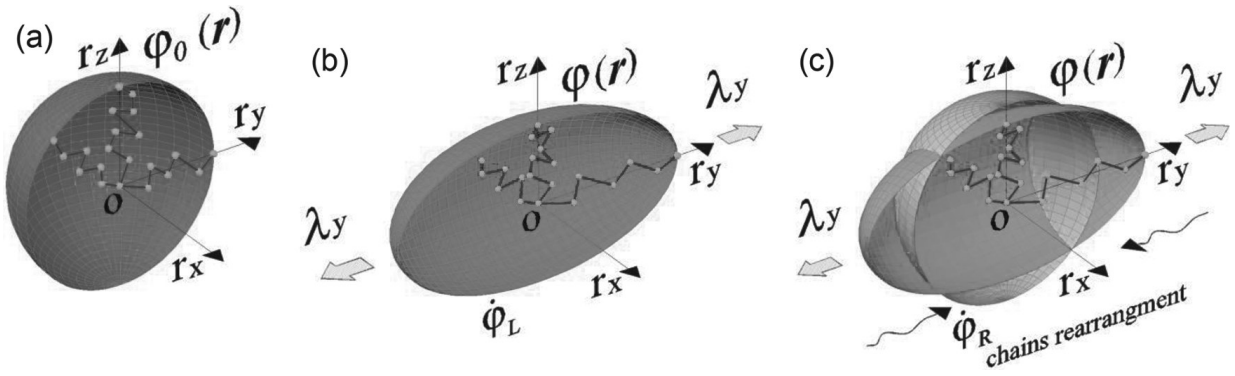

Fig. 3. (Color online) Scheme of the cross section of the chain distribution function in the chain configuration space (r_x, r_y, r_z). (a) Reference configuration in the stress-free state and (b) deformed state upon deformation in the y direction. The relaxation of the network occurs because the chains rearrange themselves in time (see Eq. (12)), making the chain distribution going back to its initial state (c). Three chains lying along the coordinate axes are indicated to underline their stretched condition.

$c_a\langle f_0(\boldsymbol{r},t)\psi(\boldsymbol{r})\rangle > 0$. Several expressions have been proposed for $\psi(\boldsymbol{r})$, such as that formulated according to the Gaussian statistics (suitable for small deformations or, equivalently, for polymer chains made of a very large number of Kuhn segments), $\psi(r) = \frac{3k_BT}{2Nb^2}|\boldsymbol{r}|^2$, or the one based on the Langevin function (valid for both moderate and large deformations) $\psi(\boldsymbol{r}) = Nk_BT\cdot\left(\frac{\phi}{bN}r + \ln\frac{\phi}{\sinh\beta}\right)$, with $\phi = \mathscr{L}^{-1}\left(\frac{r}{bN}\right)$, being $\mathscr{L}^{-1}$ the inverse of the Langevin function ($\mathscr{L}(\blacksquare) = \coth(\blacksquare) - \blacksquare^{-1}$) (Doi, 1996; Rubinstein and Colby, 2003). It is worth mentioning that the force existing in a chain is provided by $\boldsymbol{t}(N) = \partial\psi(\lambda,N)/\partial\boldsymbol{r}$, where the dependence on the deformation λ and on the number N of Kuhn's segments in the chain has been emphasized (Doi, 1996). We underline here that in the rest of the paper the hypothesis of affine deformation will be adopted, i.e. the polymer's chains are assumed to take the same deformation λ of the continuum to which they belong to.

Let us now assume the variation in time of the distribution function to be additively decomposed into the variation induced by the mechanical deformation $\dot{\varphi}_L$ (here quantified by the deformation rate gradient $\boldsymbol{L} = \dot{\boldsymbol{F}}\boldsymbol{F}^{-1}$, being $\boldsymbol{F} = \partial\boldsymbol{x}/\partial\boldsymbol{X}$ the deformation gradient tensor), and that related to the microstructure rearrangement $\dot{\varphi}_R$, as follows:

$$\dot{\varphi}(\boldsymbol{r},t) = \dot{\varphi}_L(\boldsymbol{r},t) + \dot{\varphi}_R(\boldsymbol{r},t) \tag{10}$$

It is worth mentioning that, the time variable we are considering here is not related to that of the photopolymerization process (finished at $t = t_c$). In fact, we adopt a staggered scheme with the mechanical problem starting at the new time variable $t = 0$, i.e. when the photopolymerization problem is assumed to be completed.

The two above contributions are explicitly given by (Vernerey et al., 2017):

$$\dot{\varphi}_L(\boldsymbol{r},t) = -(\nabla\varphi\otimes\boldsymbol{r} + \varphi\boldsymbol{1}) : \boldsymbol{L} \tag{11a}$$

$$\dot{\varphi}_R(\boldsymbol{r},t) = c_a\,\dot{f}_R(\boldsymbol{r},t) = k_a(c_t - c_a)f_0 - c_a[k_d + L_{ii}]f(\boldsymbol{r},t) \tag{11b}$$

where it has been assumed that the chain concentration c_a does not change in time because we are now considering the dynamic network to be at the steady state (see below); moreover, the material is assumed undergoing only isochoric deformations (incompressibility constraint), i.e. the total chain concentration does not change in time, $Dc_t/Dt = 0$ (see below) or, equivalently, at the continuum level we have $L_{ii} = 0$. In Eq. (11b) k_d, k_a are the so-called chain dissociation and association rates, quantifying how many chains per unit time detach from the current network and reattach into the stress free configuration, respectively (Vernerey et al., 2017); k_d can be also interpreted as the inverse of the relaxation time τ_r of the material. Finally, by assuming that the chain network in the stress-free condition is at the steady state (this hypothesis is assumed from now on), we have $c_a = c_{a0} = c_\mu$, where c_μ is the chain concentration related to the shear modulus μ of the material through the equation $c_\mu = \mu/(K_BT)$ (Doi, 1996); such a quantity will be evaluated according to the photopolymerization process, see Eq. (5). On the other hand, the total number of chains per unit polymer volume c_t, irrespectively of the attached or detached state of a chain, can be determined from the steady state condition, leading to $c_t = c_a(k_a + k_d)/k_a$ (Vernerey et al., 2017); by substituting in Eq. (11b), we finally obtain the following simple expression for the evolution of the chain distribution function due to the microstructure rearrangement:

$$\dot{\varphi}_R(\boldsymbol{r},t) = -k_dc_a[f(\boldsymbol{r},t) - f_0] = -k_d[\varphi(\boldsymbol{r},t) - \varphi_0] \tag{12}$$

As recalled above, when the polymer is incompressible, $tr\boldsymbol{L} = \boldsymbol{1} : \boldsymbol{L} = 0$ and Eq. (11a) simplifies to $\dot{\varphi}_L(\boldsymbol{r},t) = -\varphi_{,i}r_j\,L_{ij} = -\mathrm{div}(\varphi\dot{\boldsymbol{r}})$. The scheme of the distribution function evolution is shown in Fig. 3.

From Eq. (10), the actual chain distribution function can be easily obtained by the integration of $\dot{\varphi}(\boldsymbol{r},t)$ over time, $\varphi(\boldsymbol{r},t) = \varphi_0(\boldsymbol{r}) + \int_0^t \dot{\varphi}(\boldsymbol{r},t)dt$, allowing the corresponding actual stored deformation energy $\Delta\Psi(t)$ given by Eq. (9) to be evaluated. Finally, the

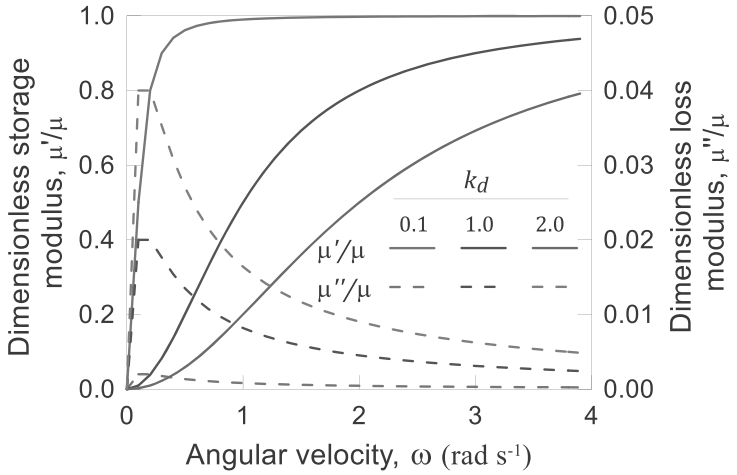

Fig. 4. (Color online) Dimensionless storage (μ'/μ) and loss modulus (μ''/μ) for different values of the chains detachment rate k_d.vs the angular velocity ω of the viscous test.

mechanical stress in the material is obtained as follows:

$$\boldsymbol{P}(t) = \frac{\partial \Delta\Psi(t)}{\partial \boldsymbol{F}} + Jp(t)\boldsymbol{F}^{-T} \tag{13}$$

where $\boldsymbol{P}$ is the (nominal) first Piola stress, and p is the hydrostatic pressure, here used as a Lagrange multiplier to ensure the incompressibility condition, mathematically expressed by $J = \det\boldsymbol{F} = 1$. Correspondingly, the true Cauchy stress $\boldsymbol{\sigma} = J^{-1}\boldsymbol{P}\boldsymbol{F}^T$, referred to the actual deformed state, is expressed as (Brighenti and Cosma, 2020):

$$\boldsymbol{\sigma} = J^{-1}\boldsymbol{P}\boldsymbol{F}^T = \left\langle c_\mu[f(\boldsymbol{r},t) - f_0(\boldsymbol{r})]\left[\frac{\partial \psi}{\partial \boldsymbol{r}} \otimes \boldsymbol{r} - k_d \psi \boldsymbol{L}^{-T}\right]\right\rangle + p\boldsymbol{1} \tag{14}$$

where $p\boldsymbol{1}$ represents the hydrostatic portion of the stress state.

As recalled above, we assume the chains to be formed during the photopolymerization to be in the stress-free reference configuration; this implies that as the photopolymerization is in progress, the distribution function changes only because the chain concentration $c_a(t)$ evolves, i.e. $\varphi_0(\boldsymbol{r}, t) = c_a(t) \cdot f_0(\boldsymbol{r})$, $t \le t_c$, while the normalized distribution $f_0(\boldsymbol{r})$ maintains the same mathematical expression. Accordingly, the energy density of the material during the photopolymerization, $\Psi(t) = c_a(t)\langle f_0(\boldsymbol{r},t)\psi(\boldsymbol{r})\rangle$, $t \le t_c$, increases as the chains are formed.

3.2. Rheology of a dynamic network

The viscoelastic nature of the mechanical response typically shown by polymers, whose strain rate-dependent response greatly affects the deformation of the material as the time goes by, is fundamental to properly design elements to be used in load bearing applications.

Classical approaches quantifying the viscous response of materials, formulated through rheological schemes based on the well-known Maxwell or the generalized Maxwell models, consider various combination of elastic spring and damper elements (Coleman and Noll, 1961).

Because of their microstructure made of long chemical chains, in polymers Brownian motions are responsible for diffusion processes, leading to the viscoelastic behavior characterized by an elastic and viscous time-dependent response. While in an ordered solid elasticity arises because of bond stretching along crystallographic planes, viscoelasticity in polymers, which is typically strongly temperature-dependent, arises from the diffusion of molecules inside an amorphous structure (Williams, 1975).

In some cases, molecular entanglements occurring in polymers during flow lead to an increase of the viscosity with the deformation rate, a phenomenon known as shear-thickening: in slow shear deformation the material behaves like a Newtonian fluid characterized by a constant viscosity, while a shear rate increase causes a nonlinear increase of the viscosity until a maximum is attained at a critical shear rate (Laun et al., 1991; Lalitha Sridhar and Vernerey, 2018). Henceforth, we neglect the above-mentioned influence of the shear rate on the polymer viscosity, and we simply assume a Newtonian-like behavior.

As mentioned above, an effective alternative to classical rheological models is provided by approaches based on the physical description of the microscale mechanisms involving a rearrangement of the material's microstructure due to reciprocal chains sliding, friction, etc. These mechanisms are also responsible for energy loss and so the dissipative character of the viscous mechanical response can be recovered. In fact, such an internal microstructure remodeling is responsible for energy dissipation due to the gradual rearrangement of the network's chains that, as usually occurs in a viscoelastic fluid, under a constant deformation gradually tend to relax their stress state.

This approach has several advantages since the evaluation of convolution integrals over the deformation history, typically required by the rheological models, can be avoided; moreover, the parameters involved in the rearrangement mechanism assume a clear physical meaning and can be easily determined. As a matter of fact, the so-called material's relaxation time is given by $\tau = 1/k_d$ and so the chains detachment rate k_d can be estimated from simple rheology experiments. According to the classical rheological models, the so-called storage and loss modulus μ' and μ'' can be defined by using the above-mentioned material's relaxation time; they are expressed in function of the chain detachment rate k_d as follows (Lewandowski and Chorążyczewski, 2010):

$$\mu' = \mu \frac{k_d^{-2}\omega^2}{1 + k_d^{-2}\,\omega^2},\ \mu'' = \mu \frac{k_d\,\omega}{1 + k_d^{-2}\,\omega^2} \tag{15}$$

where ω is the angular frequency of the oscillatory rheological test. In Fig. 4 the dimensionless storage and loss moduli are represented vs the angular velocity ω for different values of the rate k_d; low k_d values correspond to a material with a long relaxation time for which the storage modulus quickly reaches that of the fully elastic material. On the other hand, high values of the detachment rate k_d correspond to short relaxation times, leading to a material whose loss modulus rapidly increases with ω; eventually, it can even become greater than the storage modulus.

According to (Marrucci et al., 1993; Xu et al., 2010), the relaxation time can be defined as follows:

$$\tau_r = \frac{N\,b^2}{a^2}\,k_d^{-1} \tag{16}$$

where $a = c_a^{-1/3}$ is the average spatial distance of the chains. Let us now define the relaxation time $\overline{\tau}_r$ for a polymer obtained through the photopolymerization process in which the fully cured condition ($\varrho = 1$) is assumed to be reached:

$$\overline{\tau}_r = \overline{c}_a^{\,2/3}\overline{N}\,b^2\,\overline{k}_d^{-1} \tag{17}$$

In this situation, we are dealing with a polymer containing the maximum number of active chains per unit volume, $\overline{c}_a$, the minimum average value of the number $\overline{N}$ of Kuhn segments per chain and, correspondingly, the maximum relaxation time, or equivalently, the minimum value of the chains detachment rate $\overline{k}_d$. On the other hand, when a partially photopolymerized polymer is considered (i.e. a polymer that did not reach the fully cured condition), its relaxation time can be expressed as $\tau_r = c_a^{2/3} N\,b^2\,k_d^{-1}$.

A high value of the degree of cure entails the formation of a large number of cross-links per unit volume, so the number of Kuhn segments per chain is lower than that of a partially cured polymer, i.e. $N > \overline{N}$: as a consequence, the ratio $\overline{N}/N$ can be reasonably considered to be proportional to the inverse ratio of the chain concentrations, $c_a/\,\overline{c}_a$, thus providing:

$$\tau_r = \left(\frac{c_a}{\overline{c}_a}\right)^{\frac{1}{3}} \frac{k_d}{\overline{k}_d}\,\overline{\tau}_r \cong \left(\frac{c_a}{\overline{c}_a}\right)^{\frac{1}{3}} \overline{\tau}_r \tag{18}$$

Moreover, it is worth mentioning that the detachment rate of the partially photopolymerized polymer, k_d, can be reasonably assumed to be identical to that of the fully cured material, $\overline{k}_d$, being such a parameter mainly related to the temperature at which the material is deformed. From a mechanics standpoint, it must be also recalled that k_d usually depends on the stress value present in the network chains (Vernerey et al., 2017), since high stress levels promote a faster dissociation rate; for sake of simplicity, we neglect such a dependence by assuming the chains not too much stretched so, correspondingly, the chain force is not too large. Under this hypothesis, the temperature of the material mainly governs the detachment phenomenon; however, we consider an isothermal deformation in order to neglect the further dependence on the temperature.

In order to perform the parametric analyses related to the optimization of the rheological behavior (aimed at reaching the largest possible value of the relaxation time in order to minimize the viscoelastic deformation, see Sect. 6.3) of a photopolymerized polymer, in the following sections we adopt the value of the relaxation time $\overline{\tau}_r$ of the fully cured polymer as the reference for evaluating dimensionless quantities. Being the relaxation time different at each material point of the domain, for sake of simplicity we evaluate for a given curing time $t_c = w/v$ its average value within the volume V of the printed element as follows:

$$\widetilde{\tau}_r(t_c) = \frac{1}{V}\int_V \tau_r(\boldsymbol{X}, t_c)\,dV = \frac{1}{V}\frac{\overline{\tau}_r}{\overline{c}_a^{\,1/3}}\int_V c_a^{1/3}(\boldsymbol{X}, t_c)\,dV \tag{19}$$

We will use such an average quantity in the optimization problem presented in the last part of Sect. 6.3.

4. Optimal printing of a photopolymerized polymeric element

4.1. Definition of the optimization problem

In this section, we consider the problem of the optimal printing of a photopolymerized element with respect to different objective functions. The goal of the present optimization problem is finding the optimal way to obtain the utmost benefit from the available resources; as a matter of fact, the purpose of optimizing an additively manufactured material is to obtain a structural element with the best mechanical functionality by assuming, for instance, the condition of the minimum energy required for solidifying the material (i.e.

for printing). To this end, proper objective functions to be minimized are required.

In particular, firstly we consider the problem of minimizing the compliance of a structural element (for given boundary conditions), while minimizing the energy $\mathscr{E}$ required for solidifying the polymer. To this purpose, we introduce the following objective function $h_{1\alpha}$ to be minimized:

$$h_{1\alpha}(v, I_m) = \frac{\delta^*(v, I_m) - \overline{\delta}^*}{\delta^*(v, I_m)} + \alpha \ \frac{\mathscr{E}(v, I_m)}{\mathscr{E}^*} = \delta'(v, I_m) + \alpha \ \mathscr{E}'(v, I_m) \tag{20}$$

where the first term is the relative dimensionless displacement at a representative point of the solid (directly related to the element's compliance), being $\overline{\delta}^*$ the displacement taking place at the same point of the structural element made of the fully cured material, and the second one represents the normalized energy required for printing the whole domain; in Eq. (20), α is a weight parameter introduced to adjust the relative importance of the energy consumed with respect to the compliance of the element being studied.

A second optimization problem, relevant to the production of photopolymerized polymeric parts, consists in maximizing the average relaxation time of the material (i.e. the lowest degree of the viscous behavior of the material is sought) while minimizing the energy required for printing; the minimization of the following objective function guarantees the fulfilling of the above stated requirements:

$$h_{2\beta}(v, I_m) = \left[1 - \frac{\widetilde{\tau}_r(v, I_m)}{\overline{\tau}_r}\right] + \beta \frac{\mathscr{E}(v, I_m)}{\mathscr{E}^*} = \ \tau_r'(v, I_m) + \beta \ \mathscr{E}'(v, I_m) \tag{21a}$$

$$\text{being} \quad \frac{\widetilde{\tau}_r(v, I_m)}{\overline{\tau}_r} = \frac{\int_V c_a^{1/3}(\boldsymbol{X}, v, I_m) dV}{V \ \overline{c}_a^{\,1/3}} \tag{21b}$$

where β is a parameter introduced for weighting the dimensionless energy-related term with respect to the viscosity-related one.

4.2. Energy required by the photopolymerization process

In any additive manufacturing process, an important requirement consists in limiting the energy consumption of the processes, i.e. the energy necessary for photopolymerizing the material is required to be reduced at the minimum level. The energy rate irradiated to the material domain, $\dot{\mathscr{E}}(t)$, and the total amount of energy used in the process, $\mathscr{E}$, are given by:

$$\dot{\mathscr{E}}(t) = I_m \int_0^{\mathrm{w}} g(X_0, X, \ t) \ dX, \ \text{with } I_{min} \leq I_m \leq I_{max} \tag{22a}$$

$$\mathscr{E} = \int_0^{t_c} \dot{\mathscr{E}}(t) \ dt, \ \text{with } t_c = w \Big/ v \tag{22b}$$

respectively, being t_c the curing time, i.e. the time required by the light source to travel along the whole width w of the region to be solidified (Fig. 2). Since the supplied energy is converted into chemical bonds between reactant species at the micro-scale (thus reflecting in the conformation of the polymeric network at the mesoscale), the energy effectively stored in the polymerized material, $\mathscr{E}_p(v, I_m)$, can be measured by evaluating the total number of cross-links formed within the polymer; in fact, the cross-link density provided by Eq. (3) depends on the degree of cure (see Eq. (2)), which in turn depends on the amount of monomer molecules converted into polymer chains through the differential relations reported in Eqs (4a)-(4c). Thus, we can write

$$\mathscr{E}_p(v, I_m) \propto \frac{1}{\overline{c}_a} \left[\frac{1}{V} \int_V c_a(\boldsymbol{X}, v, I_m) \ dV\right] = \frac{C_a(v, I_m)}{\overline{c}_a} \leq \mathscr{E} \tag{23}$$

where $\overline{c}_a$ is the total amount of chains present in the unit printed volume of a fully cured polymer and the term in square brackets represents the average number of chains per unit volume of the actual printed polymer. It is worth mentioning that the total number of chains in the considered domain, $C_a(v, I_m) = 1/V \int_V c_a(\boldsymbol{X}, v, I_m) \ dV$, represents the level of solidification reached in the material, which depends – at a given point – on both the light intensity and on its time duration related, respectively, to the quantities I_m and v characterizing the printing process (see Fig. 2). However, the energy $\mathscr{E}_p$ does not account for the total energy spent for printing, which is instead represented by $\mathscr{E}$, but accounts only for the energy stored in the material through the formation of the chain bonds; the irradiated energy not used in the polymerization process is thus neglected in $\mathscr{E}_p$. For the above-mentioned reason, in the following the total amount of energy spent for printing will be considered in the minimization problem.

In Fig. 5 the dimensionless average chain density reached during the photopolymerization process vs time is represented for different printing velocities and maximum laser intensities. It can be noticed that the average amount of chains formed in the polymer during the photopolymerization process is greater for slower printing velocities and higher light intensities (Fig. 5a,b), while, for the

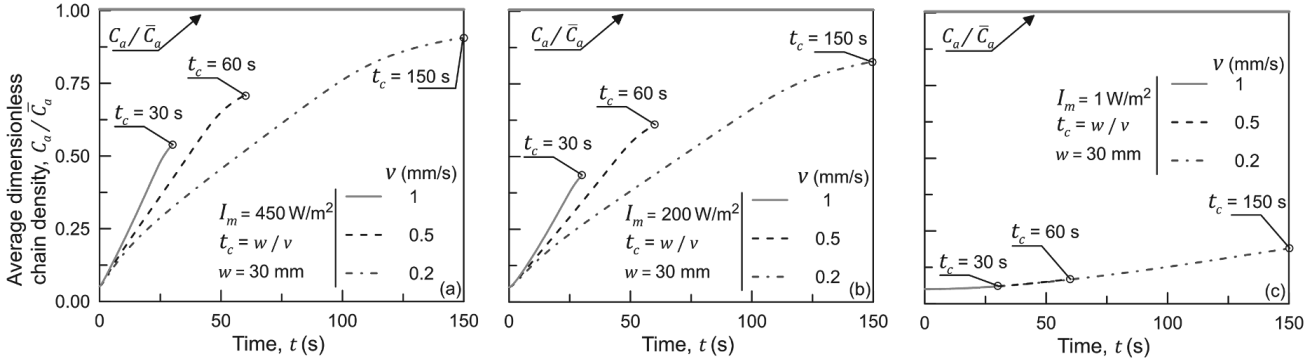

Fig. 5. (Color online) Time evolution of the dimensionless average chain density $C_a/\bar{C}_a$ for different light intensities I_m and printing velocities v (a, b, c).

same curing time, no difference can be appreciated if the laser intensity is low enough (Fig. 5c), i.e. the laser velocity does not play a role in such a case.

The quality of the printed part can thus be optimized by controlling the printing process through a proper combination of the velocity v and the maximum light intensity I_m (for sake of simplicity, we assume that the light intensity distribution function is given by the Gaussian function with a fixed standard deviation) as it will be considered in the following.

4.3. Solution of the mechanical-energetic optimization problem

Algorithms developed for unconstrained gradient-based optimization problems can be conveniently applied to solve the above-defined optimal problem (Nocedal and Wright, 2006; Kegl et al., 2002). The solution of the minimization problem can be tackled by adopting, for instance, the modified Newton's method which operates by performing a line search along the so-called *Newton direction*. It requires us to select a starting point in the solution space, in our case represented by the variables v, I_m collected in the vector $\boldsymbol{\xi} = (v, I_m)$; the design variables are iteratively updated, i.e. $\boldsymbol{\xi}_k = (v_k, I_{mk})$ where $k = 0, 1, 2, \ldots n$ is the iteration number. The procedure requires the gradient $\boldsymbol{d}_i(\xi_k) = \nabla h_i(\boldsymbol{\xi}_k)$ $(i = 1,\ 2)$ of the objective function at the point $\boldsymbol{\xi}_k$ to be evaluated for the optimization problem to be solved. If the objective function is sufficiently regular and has a global minimum, when the norm of the gradient fulfills the convergence criterion, $\| \boldsymbol{d}_i(\boldsymbol{\xi}_k)\| \leq \epsilon$ (being ϵ a sufficiently small convergence tolerance) the optimal point is reached. The solution can be obtained by an iterative procedure where the Hessian of the objective function, $\boldsymbol{H}_i(\boldsymbol{\xi}_k) = \nabla^2 h_i(\boldsymbol{\xi}_k)$, is used to find the search direction $\boldsymbol{p}_i(\boldsymbol{\xi}_k)$:

$$\boldsymbol{p}_i(\boldsymbol{\xi}_k) = -\boldsymbol{H}_i^{-1}(\boldsymbol{\xi}_k)\ \boldsymbol{d}_i(\boldsymbol{\xi}_k) \tag{24}$$

In order to update the solution in the solutions space, the step length γ_k to be used along the above direction $\boldsymbol{p}_i(\boldsymbol{\xi}_k)$ has to be defined according to the condition: $h_i(\boldsymbol{\xi}_k + \gamma_k\, \boldsymbol{p}_i(\boldsymbol{\xi}_k)) < h_i(\boldsymbol{\xi}_k)$.

The vector $\boldsymbol{\xi}_k$ of the design variables is then updated as follows $\boldsymbol{\xi}_{k+1} = \boldsymbol{\xi}_k + \gamma_k\, \boldsymbol{p}_i(\boldsymbol{\xi}_k)$, and the solution continues by evaluating the new quantities $\boldsymbol{d}_i(\xi_{k+1})$, $\boldsymbol{H}_i(\boldsymbol{\xi}_{k+1})$ and $\boldsymbol{p}_i(\boldsymbol{\xi}_{k+1})$ until the required convergence criterion is fulfilled.

5. Numerical implementation of the multiphysics model

The above presented multi-physics problem involving the chemical-physics photopolymerization process and the mechanics of the obtained viscoelastic materials, is suitable to be efficiently implemented in a finite element (FE) framework. The light diffusion process, together with the photo–induced polymerization, and the mechanical problem can be solved in a staggered way by assuming the mechanical part of the problem to follow the initial production process of the material. By introducing the weak form – expressed by Eq. (25a) – of the light diffusion governing equations (Eq.(6)), and adopting a standard FE interpolation (see Eq. (25b)) of the quantities of interest (■) through the use of their nodal values (■$_i$), the following discretized form of the problem, Eq. (25c), is obtained:

$$\int_{\partial\Omega_0} \mathfrak{w}(\boldsymbol{X})\ I(\boldsymbol{X},\ t)\ \bar{\boldsymbol{l}}(\tau)\cdot\boldsymbol{n}\ dS = I_0 \int_{\partial\Omega_0} \mathfrak{w}(\boldsymbol{X})\ g(\boldsymbol{X},\ t)\ l_n\ dS \tag{25a}$$

$$\begin{aligned} I_h(t) &= \sum_{i=1}^{n_n} N_i I_i(t), \quad \nabla_X I_h(t) = \sum_{i=1}^{n_n} [B]_i I_i(t), \\ \mathfrak{w}_h &= \sum_{i=1}^{n_n} N_i \mathfrak{w}_i, \qquad \nabla_X \mathfrak{w} = \sum_{i=1}^{n_n} [B]_i \mathfrak{w}_i \end{aligned} \tag{25b}$$

$$[\boldsymbol{E}(t) + \boldsymbol{A}(t) + \boldsymbol{D}]\ \boldsymbol{I}(t) = \boldsymbol{Q}(t) \tag{25c}$$

Table 1
Governing equations of the multi-physics problem of the mechanics of a photopolimerized polymeric material.

	Eq. No.	Meaning	Eq. Expression	Parameters
Photopolymerization problem	(1)	Chemical reactions taking place during the photopolymerization	$Ph_I \overset{k_{pr}}{\rightarrow} 2R^\bullet$, $R^\bullet + M \overset{k_p}{\rightarrow} P^\bullet$, $P^\bullet + M \overset{k_p}{\rightarrow} P^\bullet$ $P^\bullet + P^\bullet \overset{k_t}{\rightarrow} P_{\text{dead}}$, $P^\bullet + R^\bullet \overset{k_t}{\rightarrow} P_{\text{dead}}$	$m,\ k_{pr}, k_t,\ k_p$
	(6)	Beer-Lambert light diffusion eq. and related Dirichlet B.C.	$l(\boldsymbol{X},\ t) \cdot \nabla_X I(\boldsymbol{X},\ t) = -A(\boldsymbol{X},\ t)\, I(\boldsymbol{X},\ t)$ $I(\boldsymbol{X},\ t) = \bar{I}(\nu,\ I_m, t)$	$A(\boldsymbol{X},\ t), \nu,\ I_m,$ $t \le t_c$
	(4)	Rates of the photoinitiator, free radicals and monomer concentration, respectively	$\dot{C}_I(\boldsymbol{X},t) = -k_{pr}\, I(\boldsymbol{X},t)\, C_I(\boldsymbol{X},t)$ $\dot{C}_R(\boldsymbol{X},t) = -m\, \dot{C}_I(\boldsymbol{X},t) +$ $- m\, k_t(\boldsymbol{X},t)[C_R(\boldsymbol{X},t)]^2$ $\dot{C}_M(\boldsymbol{X},t) = -k_p(\boldsymbol{X},t) C_M(\boldsymbol{X},t) C_R(\boldsymbol{X},t)$	$m,\ k_{pr}, k_t,\ k_p, t \le t_c$
		Evolution of the monomer concentration	$C_M(\boldsymbol{X},t) = C_{M0} + \int_0^t \dot{C}_M(\boldsymbol{X},\tau)\, d\tau$	$t \le t_c$
	(2)	Current value of the degree of cure	$\varrho(\boldsymbol{X},t) = 1 - \dfrac{C_M(\boldsymbol{X},t)}{C_{M0}(\boldsymbol{X})}$	$t \le t_c$
	(5)	Chain concentration	$c_a(\boldsymbol{X},t) = \dfrac{\overline{\mu}}{k_B T} \cdot \exp[\varpi(\varrho(\boldsymbol{X},t) - 1)]$ $c_{a0}(\boldsymbol{X}) = c_a(\boldsymbol{X}, t_c)$	$\overline{\mu}, k_B, T,\ \varpi, t \le t_c$
Mechanical problem	(11a)	Distribution function rate due to deformation	$\dot{\varphi}_L(\boldsymbol{r},t) = -(\nabla\varphi \otimes \boldsymbol{r} + \varphi 1) : \boldsymbol{L}$	$t \ge t_c$
		Distribution function rate due to the viscous effect	$\dot{\varphi}_R(\boldsymbol{r},t) = -k_d c_{a0}(\boldsymbol{X})(f(\boldsymbol{r},t) - f_0)$	$k_d,\ c_{a0}(\boldsymbol{X}), t \ge t_c$
	(9)	Energy density of the material	$\Delta\Psi(\boldsymbol{X},t) = \Psi(\boldsymbol{X},t) - \Psi_0(\boldsymbol{X}, t=0) =$ $c_{a0}(\boldsymbol{X}) \Delta f(\boldsymbol{r},t)\ \psi(\boldsymbol{r})$	$c_{a0}(\boldsymbol{X}), t \ge t_c$
	(13)	Nominal stress tensor determination	$\boldsymbol{P}(\boldsymbol{X},t) = \dfrac{\partial \Delta\Psi(\boldsymbol{X},t)}{\partial \boldsymbol{F}} + Jp(t)\boldsymbol{F}^{-T}$	$t \ge t_c$

In (25a) $\mathbb{w}$ represents a test function, while $[N]$, $[B]$ are the standard shape functions and compatibility matrix, respectively, ($\blacksquare_h$) are the interpolated quantities, while the matrices $\boldsymbol{E}, \boldsymbol{A}, \boldsymbol{D}$ are the light gradient matrix, the depletion matrix and the stabilization matrix of the discrete problem, respectively, while $\boldsymbol{Q}(t)$ is the vector of the nodal values of the incoming light intensity on the top boundary of the domain (Fig. 2) and $\boldsymbol{I}$ is the vector of the sought light intensity value at the nodes; all these nodal vector quantities are obtained by assembling the corresponding values related to the single finite element used to discretize the problem, i.e. $\boldsymbol{E}(t) = \mathbb{A}_{e=1}^{ne} \boldsymbol{E}_e(t)$, $\boldsymbol{A}(t) = \mathbb{A}_{e=1}^{ne} \boldsymbol{A}_e(t)$,$\boldsymbol{D} = \mathbb{A}_{e=1}^{ne} \boldsymbol{D}_e$,$\boldsymbol{Q} = \mathbb{A}_{e=1}^{ne} \boldsymbol{Q}_e(t)$, and $\boldsymbol{I} = \mathbb{A}_{e=1}^{ne} \boldsymbol{I}_e$, being $\mathbb{A}$ the assembly operator and ne the number of finite elements used in the discretization. Finally, the function $g_n(\boldsymbol{X},\ t) = l_n\ g(\boldsymbol{X},\ t)$ represents the distribution of the light beam intensity normal to the boundary of the domain, being l_n the scalar product of the beam light versor and the normal to the boundary. Once at a given time instant the light intensity within the domain is known, the value of the photo-initiator concentration at the time t_i can be obtained by updating its value in time as follows

$$C_{I,\ GP}(t_i) = C_{I,\ GP}(t_{i-1}) + \Delta t \underbrace{\left[-k_{pr}\ I_{h,\ GP}(t_i) C_{I,\ GP}(t_{i-1}) \right]}_{\dot{C}_{I,\ GP}(t_i)} \tag{26}$$

where $\Delta t = (t_i - t_{i-1})$ is the time step interval adopted in the time integration procedure. In the above expression, we considered all the involved quantities referred to the generic Gauss point (GP) within a generic finite element. Correspondingly, the concentrations of the free radicals, as well as that of the monomer (see Eqs (4a)-(4b)) can be determined. Then, the pointwise value of the degree of cure $\varrho_{GP}(t_i)$ (Eq. (2)) and the related chain concentration $c_{a,\ GP}(t_i)$ (see Eq. (5)) are evaluated. Finally, for a given curing time t_c, the distribution of the shear modulus of the material at the generic Gauss point GP is provided by $\mu_{\ GP}(t_c) = k_B T c_{a,\ GP}(t_c)$.

The nonlinear mechanical problem can be solved with a standard procedure, usually adopted in geometrically and mechanically non-linear problems, consisting in finding the unbalanced nodal force vector whose component, corresponding to the $i-th$ degree of freedom of the discretized problem, is given by:

$$R_{ui} = \int_{\mathscr{B}_0} [B]_i^T \boldsymbol{P}\ dV - \left(\int_{\mathscr{B}_0} [N]_i^T \boldsymbol{B}\ dV + \int_{\partial\mathscr{B}_0} [N]_i^T \overline{\boldsymbol{T}}\ dA \right) \tag{27}$$

where the integrals have been assumed to be evaluated in the reference (undeformed) configuration of the body. In Eq. (27) $\boldsymbol{P} = \partial\Delta\Psi / \partial\boldsymbol{F} + Jp\boldsymbol{F}^{-T}$ is the first Piola stress tensor (see Sect. 3.1, Eq. (13) and related text), while $\boldsymbol{B}, \overline{\boldsymbol{T}}$ are the body applied forces and tractions, respectively, and $[B]_i$, $[N]_i$ are the compatibility and the shape function matrix, respectively, related to the $i-th$ degree of freedom. Upon linearization, the above-stated nonlinear problem can be written in incremental form and solved through the use of a standard iterative procedure (Brighenti et al., 2021).

The summary of the governing equations and the related involved parameters for both the photopolymerization as well as the mechanical problem is reported in Table 1.

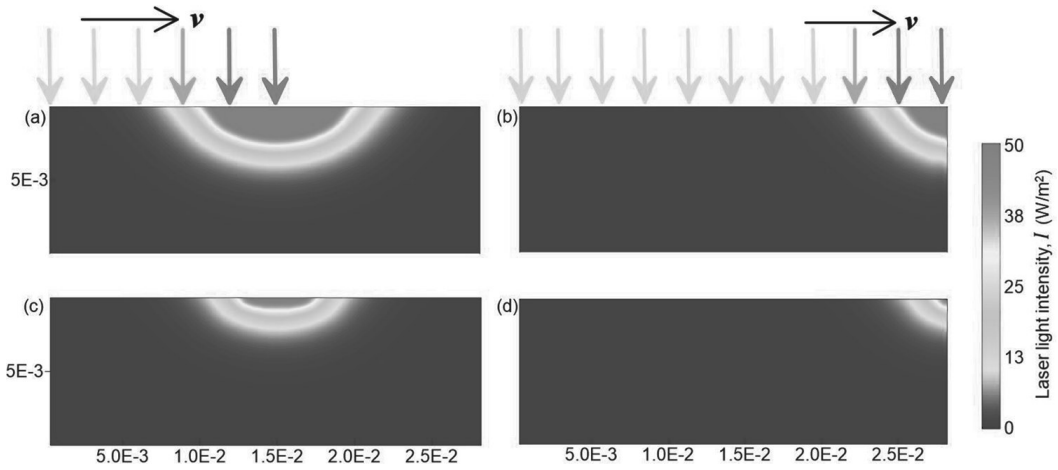

Fig. 6. (Color online) Light intensity field within the monomer being cured: case of maximum light intensity of the incoming light beam $I_m = 350\ W/m^2$ (top row) and $I_m = 100\ W/m^2$ (bottom row) at the dimensionless curing times $t^* = 0.5$ (a, c) and $t^* = 1$ (b, d). Geometrical dimensions in [m].

6. Numerical examples

In order to underline the role played by the main involved parameters on the mechanical response of a photopolimerized material, in this section we firstly apply the above-developed multi-physics model to the simulation of the photopolymerization process. Then, we consider the problem of finding the optimal combination of the printing parameters, leading to the minimization of the objective function of interest (see Sect. 4). In particular, we consider some representative simple structural elements whose response must: i) have the minimum compliance while using the minimum amount of energy for the photopolymerization, and ii) display the minimum viscous behavior while considering the same above-mentioned minimum energy requirement. For sake of simplicity, in all the examples we simulate the curing process of a liquid monomer contained in a 2D vat having thickness $h = 10\ mm$ and width $w = 30\ mm$, discretized with 12 (w) x 10 (h) four noded bilinear finite elements. The laser moves from left-to-right on the top of the liquid; for sake of simplicity and to enhance the interpretation of the results, it is assumed that a single layer of the monomer is photopolymerized, i.e. we neglect the solidification of successive layers as usually done in building an additively manufactured part. The photopolymerization process ends when the laser covers the whole width w of the layer being printed: the time required by the laser to cover such a distance is $t_c = w/v$ (curing time), while the dimensionless curing time is defined as $t^* = t/t_c$, with $0 \le t^* \le 1$. The chemical properties of the initial liquid monomer being solidified are assumed as follows: 1) initial photo-initiators concentration $C_I(\boldsymbol{X}, 0) = 20\ mol\ m^{-3}$, 2) initial liquid monomer concentration $C_M(\boldsymbol{X}, t = 0) = 3000\ mol\ m^{-3}$, 3) photo-decomposition rate $k_{pr} = 8 \cdot 10^{-4} s^2/kg$, 4) propagation and termination rates $k_P = k_T = 0.21\ m^3 \cdot s\ \cdot mol^{-1}$. In order not to introduce further complexities, the above recalled rates k_P and k_T are assumed to be constant throughout the entire photopolymerization process. Furthermore, we assume the shear modulus of the fully cured polymer obtainable from such a type of chemical resin to be $\overline{\mu} = 267\ MPa$, while we adopt $\varpi = 3$. Finally, we assume the photo-initiator molar absorptivity to be $\theta = 30\ m^2 mol^{-1}$, while the absorbance of the fully cured polymer and of a liquid monomer (assumed to be fully transparent) are $A_{pol} = 2400\ m^{-1}$ and $A_{mon} = 0\ m^{-1}$, respectively. No photoabsorbers are considered to be present in the resin, i.e. $A_{abs}(\boldsymbol{X},\ t) = 0$. Unless differently stated in the text, we assume a constant material absorbance $A(\boldsymbol{X}, t) = A_L = 600\ m^{-1}$, estimated from Eq. (7) at $t^* = 0$ i.e. when $\varrho(\boldsymbol{X},\ 0) = 0$, during the whole curing process. In other words, in the first part of this section, we assume that the resin being solidified maintains the absorbance properties of the initial liquid state during the whole curing process. The results related to a representative case characterized by a variable material's absorbance, evaluated according to the solidification evolution, will be also investigated in sect. 6.3.

6.1. Simulation of the photopolymerization process and resulting mechanical behavior

In this section we present the numerical simulation of the photopolymerization process of a liquid monomer irradiated by a laser source – characterized by various peak light intensities – moving at different translation velocities. The considered problem is modeled by adopting a 2D domain and the light intensity distribution hitting the top boundary surface of the domain is assumed to be described by the expression $I(\boldsymbol{X},\ t) = I_m \exp \frac{-(X-vt)^2}{c}$, where v is the linear (constant) velocity of the light beam, while c defines the width of the Gaussian distribution, here assumed to be $c = 10^{-6}\ m$ (Fig. 2). The following values characterizing the moving light source are assumed: $I_m = 100,\ 350\ W/m^2$ and $v = 2 \cdot 10^{-4},\ 1 \cdot 10^{-3}\ m/s$. Since the purpose of the present analyses is to underline the effects of the parameters involved in the photopolymerization process, the adopted parameters are not related to an effective liquid monomer used in 3D printing; however, the order of magnitude of the assumed values are within the range usually encountered in realistic cases (Perry and Young, 2005; Wu et al., 2018).

Fig. 6 shows the light intensity distribution at two different time instants, namely at $t^* = 0.5$ (half way of the curing) and $t^* = 1.0$ (end of the curing path) within the analyzed domain for two different maximum intensity values of the light beam.

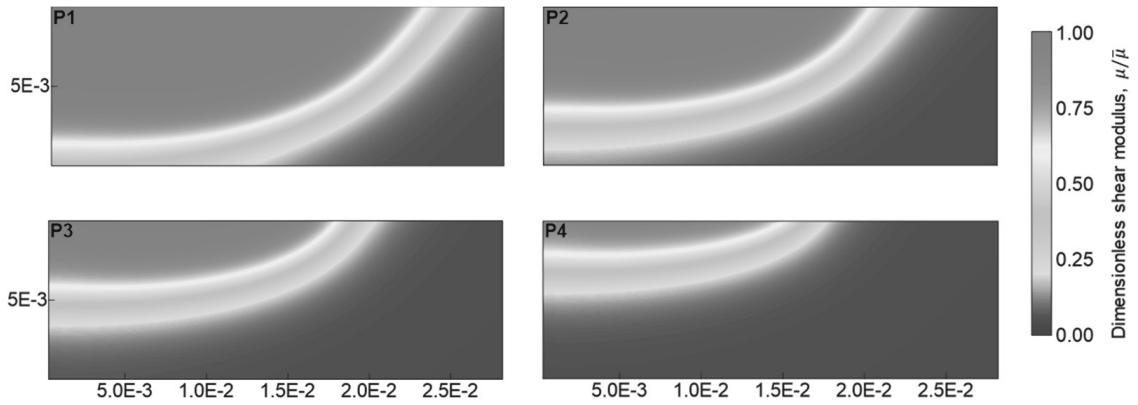

Fig. 7. (Color online) Maps of the dimensionless shear modulus obtained by photopolymerizing the liquid monomer with four different printing setups: $v = 2 \cdot 10^{-4}\ m/s$, $I_m = 350\ W/m^2$ and $I_m = 100\ W/m^2$ (P1 and P2, respectively), and $v = 1 \cdot 10^{-3}\ m/s$, $I_m = 350\ W/m^2$ and $I_m = 100\ W/m^2$ (P3 and P4, respectively). The maps are referred to the time instant $t^* = 0.5$, i.e. when the laser has covered one half of the monomer vat width w. Dimensions in [m].

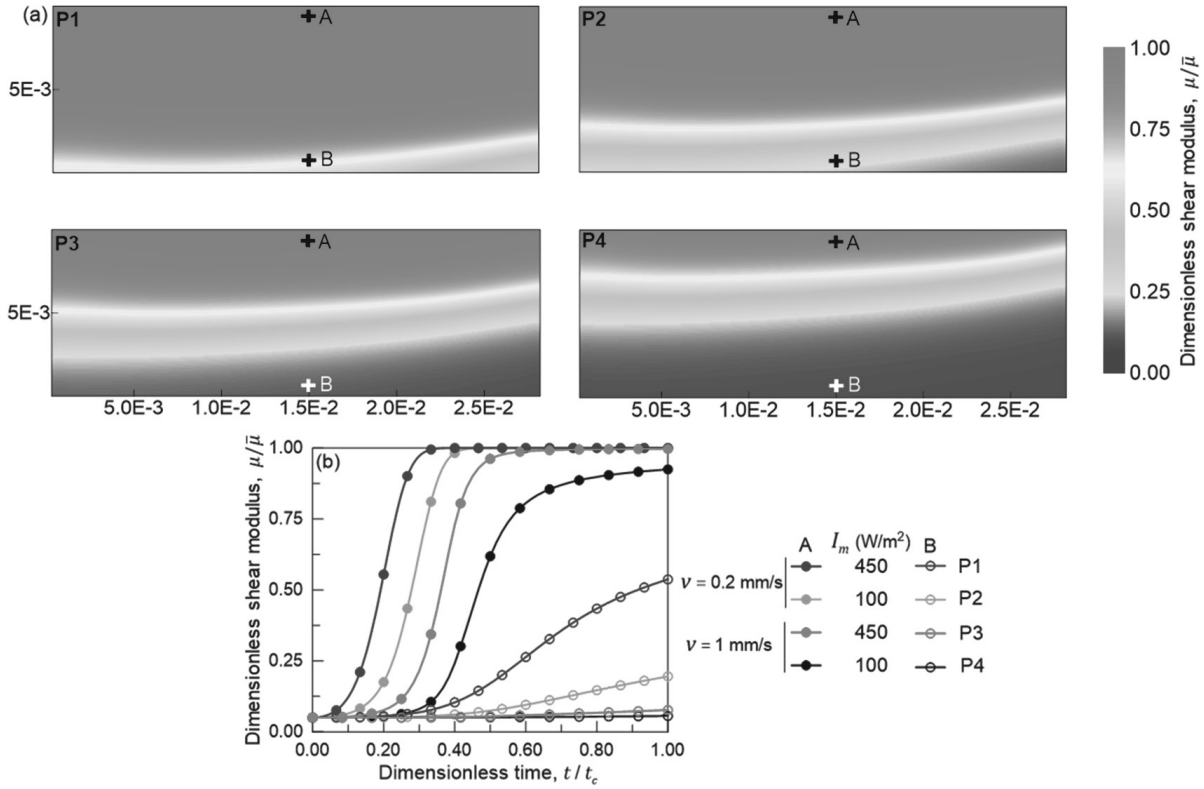

Fig. 8. (Color online) (a) Maps of the dimensionless shear modulus of the final component (i.e. at $t^* = 1$) printed with the four printing setups illustrated in Fig. 6b and Fig. 6d. Evolution of the dimensionless shear modulus during the printing process at the two points *A* and *B* placed at $\xi = 0.1$ (A) and $\xi = 0.9$ (B). Dimensions in [m].

The distribution of the dimensionless shear modulus reached in the material at $t^* = 0.5$ for two different maximum beam light intensity values and two traveling velocities, is displayed in Fig. 7.

Correspondingly, at $t^* = 1.0$ the distribution of the dimensionless shear modulus $\mu/\overline{\mu}$ for the above mentioned printing parameters, is illustrated in Fig. 8a; the evolution in time of $\mu/\overline{\mu}$ is represented in Fig. 8b at two points in the middle of the top (point A, $\xi = \eta/h = 0.1$, being $\eta = |Y|$ the distance measured from the top surface) and bottom (point B, $\xi = 0.9$) regions of the element being cured. It can be appreciated that, irrespectively of the light intensity and velocity, when the dimensionless time tends to $t^* = 1.0$ in the upper part of the element the shear modulus nearly reaches the value of the fully cured polymer (especially for the lower values of the velocity), while the degree of cure at the bottom point B is less pronounced and increases slowly in time. Since the degree of cure is the results of a kinetic chemical equilibrium, a longer irradiation time (lower light translational velocity) entails a more pronounced, homogenous and deeper degree of cure of the material.

The videos showing the light distribution evolution as well as the evolution of the dimensionless shear modulus and of the active

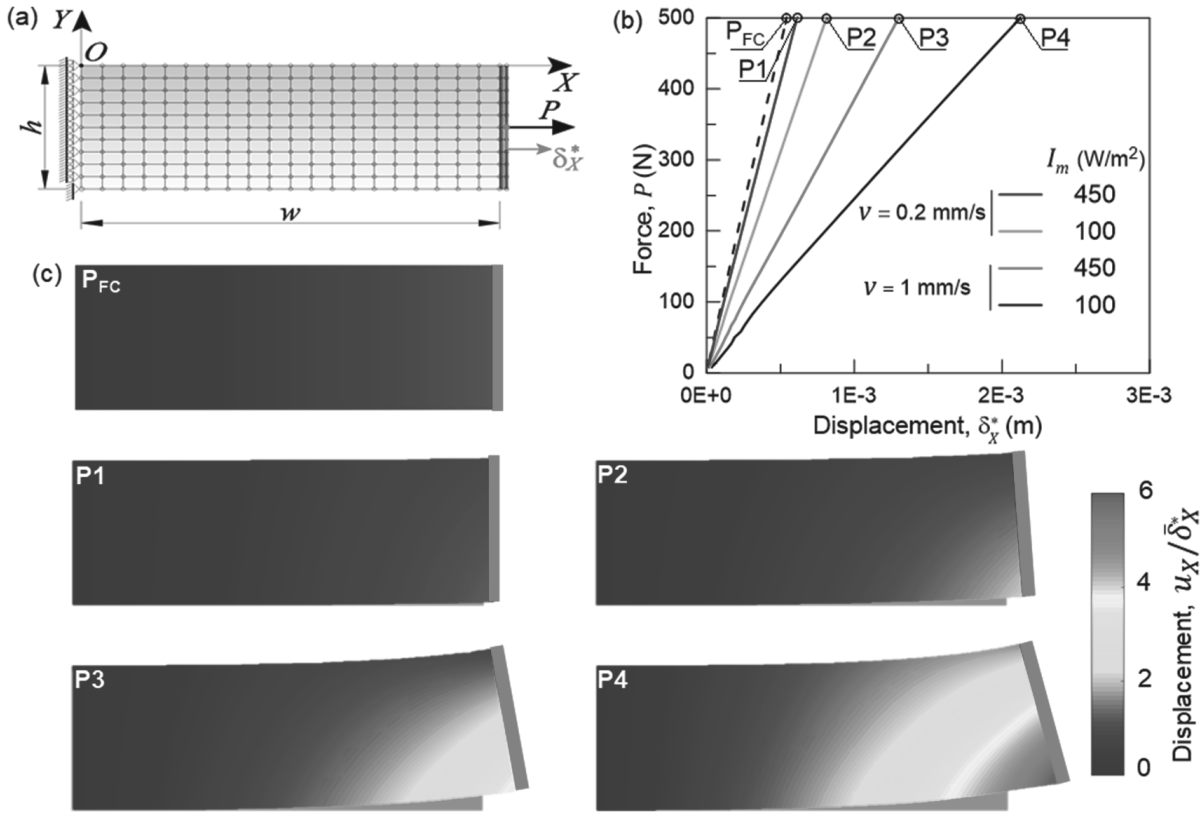

Fig. 9. (Color online) (a) Mesh of the investigated structural element and force vs central point displacement curves for four different photopolymerization setups (P1-P4) (b). (c) Dimensionless horizontal displacement fields for the fully cured component (P_{FC}) and for the components obtained by using the various setups (P1-P4 in Fig. 7). The maps have been obtained by normalizing the horizontal displacements with respect to the horizontal displacement $\overline{\delta}_X^*$ of the central point of the right edge of the fully cured structural element.

chains concentration, for a case with $I_m = 150\ W/m^2$ and $v = 1\ mm/s$, are provided in the supplementary material of this paper.

The above considered photopolymerized element is now studied from a mechanical viewpoint: the element is assumed to be stretched by a tensile force as indicated in Fig. 9a. The structural element's domain is discretized as done in the photopolymerization problem, and a rigid bar placed at $X = w$ is introduced in order to distribute the applied force over the entire height of the element. The load-displacement curves (upto the applied load intensity $P = 500\ N$) obtained through a nonlinear FE analysis performed by considering both geometric and material nonlinearities – the latter treated according to the micromechanical model presented above (see Sect. 3.1) – are illustrated in Fig. 9b. The mechanical response of the fully-cured element as well as those of the structural elements obtained by using four different photopolymerization setups (see Fig. 8) is provided. It can be appreciated that the photopolymerization process setup has a strong effect on the mechanical response, as clearly demonstrated by the deformed shape of the element, Fig. 9c. As expected, the use of the highest light intensity and of the lowest velocity leads to the better mechanical properties of the element that, in such a case, behaves similarly to the fully cured material. The non-symmetric deformation arising for the cases related to the not fully cured elements is clearly visible (Fig. 9c). In the Section 6.3, the structural element here considered will be adopted for studying the mechanical optimization problem with the energy constraint.

In order to study the influence of uncertain input parameters for a better understanding of their role in the photopolymerization process, in the last part of this section we consider the effect of uncertain light beam velocity and intensity on the final obtained mechanical characteristics (Vu-Bac et al., 2016). In Fig. 10 the effect of the uncertainty in the maximum light intensity (±5%, ±10%, ±50%) for two different light velocities (Fig. 10a, b) and the effect of the uncertainty in the light velocity (±5%, ±10%, ±50%) for two different maximum light intensities (Fig. 10c, d) are illustrated through the dimensionless shear modulus plotted along a vertical cross-section of the printed element. The variation of the dimensionless shear modulus close to the top (bottom) surface of the element is noticeably (slightly) influenced by the maximum light intensity for high light speed (Fig. 10a). The opposite occurs for the lowest light speed considered (Fig. 10b) where no remarkable effect can be appreciated.

The effect of the light velocity uncertainty on the polymer's shear modulus (Fig. 10c, d), studied for the lowest value of the maximum light intensity ($I_m = 100\ W/mm^2$), happens to be negligible at the bottom but not at the top of the domain (Fig. 10c), while for the highest value of the maximum light intensity ($I_m = 400\ W/mm^2$), it is less important at the top edge of the domain and more at the bottom (Fig. 10d).

As a general conclusion, it can be noticed that a relatively large variation in the input parameters (±10%) does not affect significantly the resulting mechanical properties of the material, thus indicating that a non perfect tuning of the photopolimerization parameters does not play a significant role in the final solidified material.

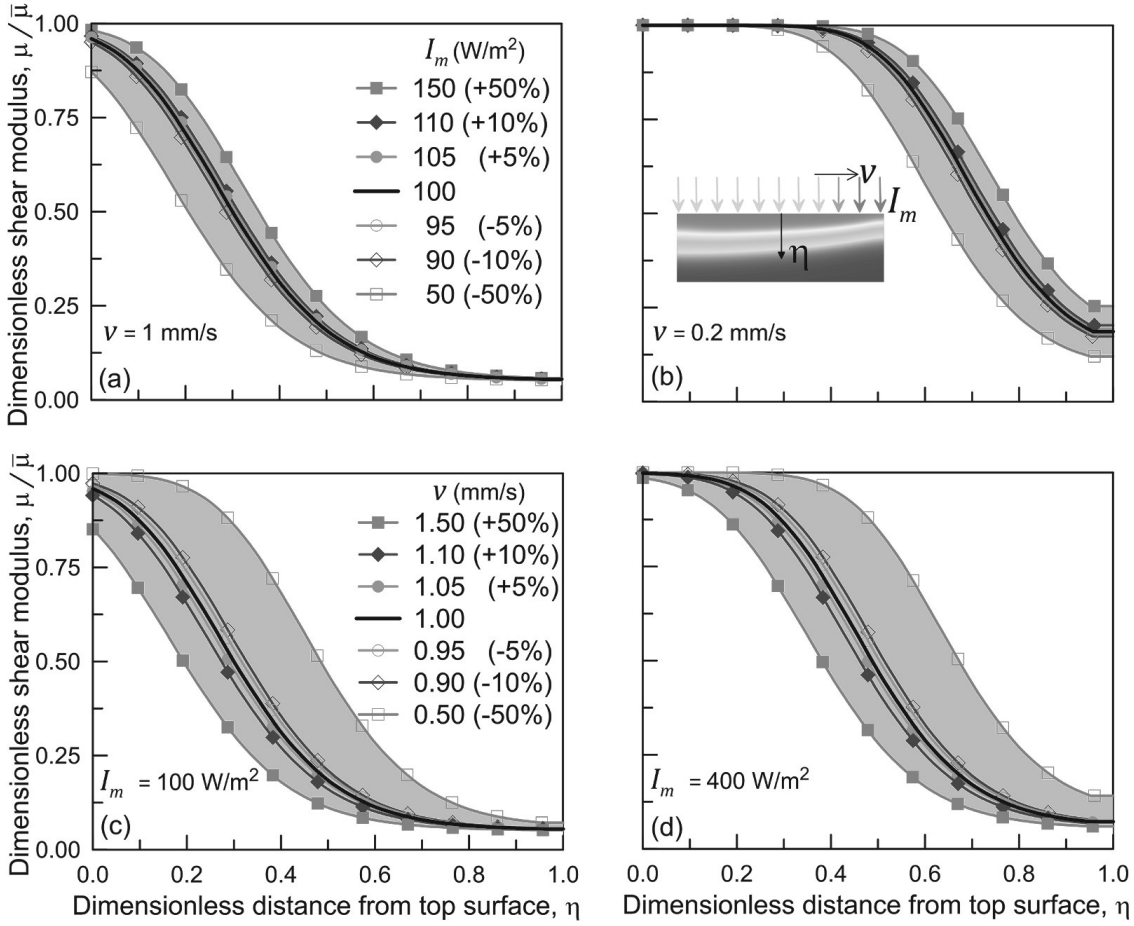

Fig. 10. (Color online) (a) Sensitivity analysis related to the uncertainty of the maximum light intensity for two different light velocities (a, b) and of the uncertainty of the light velocity for two different maximum light intensities (c, d); the dimensionless vertical coordinate $0 \leq \eta \leq 1$ has been used.

6.2. Validation of the photopolymerization model

In order to validate the proposed model describing the chemical-physics phenomena involved in the photopolymerization process, in this section we consider the simulation of a real photopolymerization process taken from the literature. All the involved parameters different from those used in the previous example are listed below. The monomer used is polyethylene (glycol) diacrylate (PEGDA) (with a molecular weight of 250 g/mol, Sigma-Aldrich, St. Louis, USA), and 0.3% weight percent 2,2-Dimethoxy-2-phenylacetophenone (Sigma-Aldrich, St. Louis, USA) as the photo-initiator. We perform the FE analyses by assuming a stationary laser beam $v \to 0\ m/s$ irradiating a single point lying on the resin surface, as made in (Wu et al., 2018). The rate parameters used for the simulations are given by

$$k_p = \frac{k_{p0}}{1 + \frac{k_{p0}}{k_{p,D0}} e^{d\varrho}} \quad \text{and} \quad k_t = \frac{1}{\frac{1}{k_{t,SD}} + \frac{e^{d\varrho}}{k_{t,TD0}}} + \frac{C_{RD}(1-\varrho)k_{p0}}{1 + \frac{k_{p0}}{k_{p,D0}} e^{d\varrho}} \tag{28}$$

for the propagation and termination rate constants, respectively. Since the presence of oxygen can induce inhibition of the photopolymerization process, we modify Eq. (4b) by taking into account the oxygen concentration $C_O(\boldsymbol{X}, t)$ since it affects the evolution of free radicals; the new relation becomes:

$$\dot{C}_R(\boldsymbol{X}, t) = -m\ \dot{C}_I(\boldsymbol{X}, t) - m\ k_t(\boldsymbol{X}, t)[C_R(\boldsymbol{X}, t)]^2 - k_O C_R(\boldsymbol{X}, t) C_O(\boldsymbol{X}, t) \tag{29}$$

where $\dot{C}_O(\boldsymbol{X}, t) = -k_O C_O(\boldsymbol{X}, t) C_R(\boldsymbol{X}, t)$ (Wu et al., 2018). According to Wu et al. (2018), we adopt the following parameters: $k_{p0} = 1.86048\ \frac{m^3}{mol\ s}$, $k_{p,D0} = 8.994 \cdot 10^8 \frac{m^3}{mol\ s}$, $k_{t,SD} = 4.39 \cdot 10^3 \frac{m^3}{mol\ s}$, $k_{t,TD0} = 10\ 024.43\ \frac{m^3}{mol\ s}$, $k_{pr} = 8.999 \cdot 10^{-4} \frac{s^2}{kg}$, $d = 34.149$ and $C_{RD} = 1.0146$.

Fig. 11 illustrates the evolution in time of the degree of cure $\varrho(t)$ provided by the model by accounting for the photopolymerization inhibition induced by the presence of oxygen (Fig. 11a) and by neglecting such an effect (Fig. 11b); when all the main influencing parameters are considered, the agreement appears to be satisfactory, while when the oxygen effect is not considered the degree of cure is over estimated and the predicted polymerization appears to occur faster (Fig. 11b).

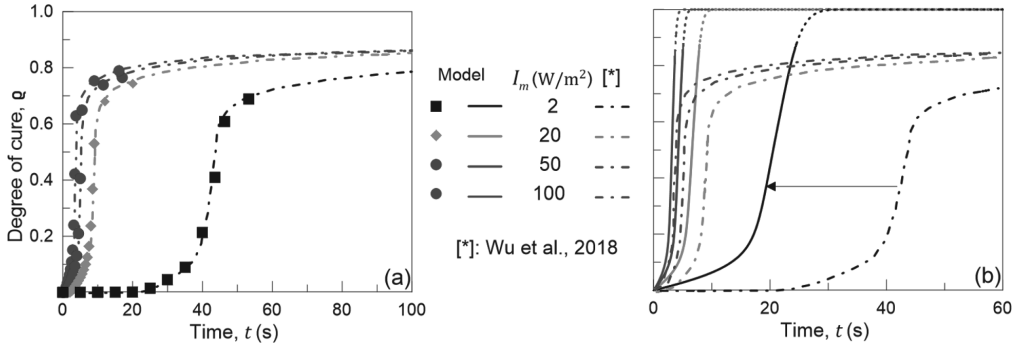

Fig. 11. (Color online) Evolution of the degree of cure estimated with the present model with (a) and without (b) the oxygen inhibition of the photopolymerization. Literature results (Wu et al., 2018) are also shown. In (b) the dashed-point curves of (a) are reported for comparison with the cases where the oxygen effect is neglected (continuous curves in (b)).

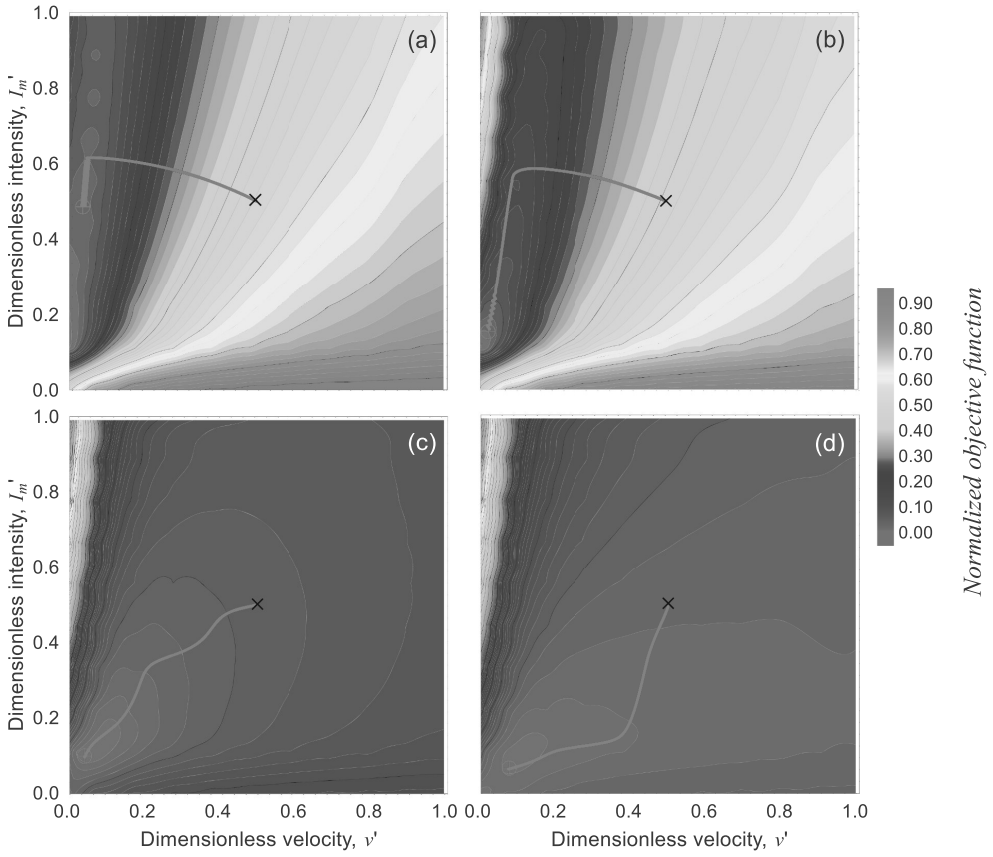

Fig. 12. (Color online) Map of the normalized objective function $h_{1\alpha}$ for different values of the parameter α: (a) $\alpha = 0.2$, (b) $\alpha = 1$, (c) $\alpha = 5$ and (d) $\alpha = 10$. Starting from the initial point ξ_0 ($\times$ assumed centered in the design domain), the solution of the optimization problem evolves as indicated by the red paths and ends at the optimal condition indicated by the symbol $\oplus$.

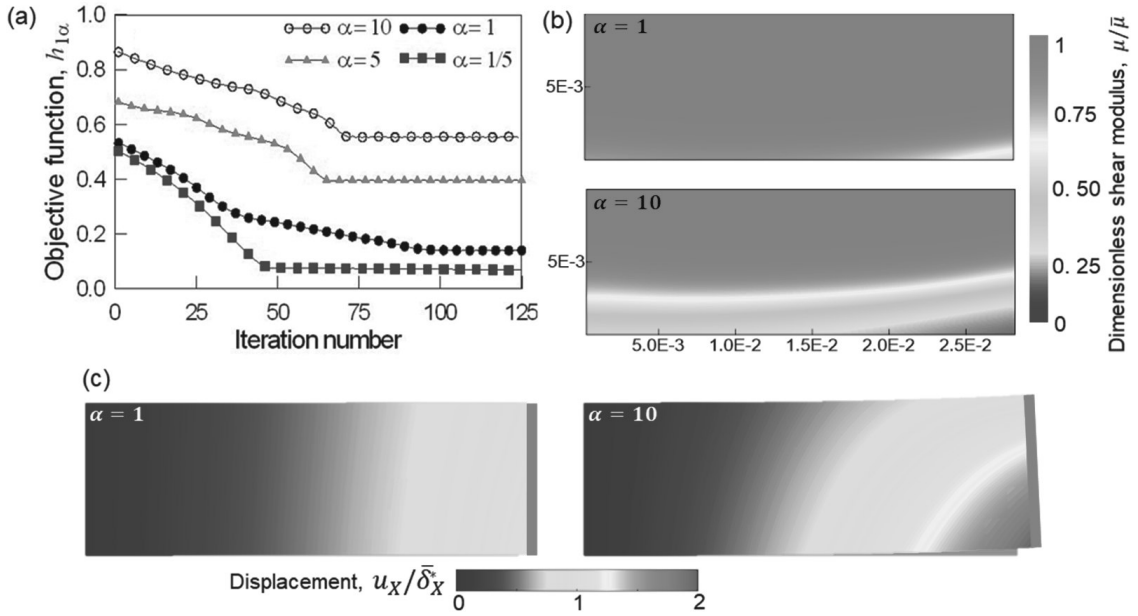

Fig. 13. (Color online) (a) Evolution of the objective function $h_{1\alpha}$ during the optimization iterations for different values of the weight parameter α. (b) Dimensionless shear modulus in the final component obtained by using the best printing values of the design parameters $\nu,\ I_m$ evaluated for $\alpha = 1$ and $\alpha = 10$. (c) Corresponding deformed shapes with color maps indicating the dimensionless horizontal displacement field. Dimensions in [m].

6.3. Optimization of the photopolymerization process with respect to the mechanical response of polymers

In the present section, we consider the problem of minimizing the objective function $h_{1\alpha}(\nu, I_m)$ (see Sect. 4.1) for a structural element undergoing mechanical actions. The objective function $h_{1\alpha}(\nu, I_m)$ (Eq. (20)) to be minimized, is aimed at minimizing at the same time the structural element's compliance and the energy required for its solidification, the latter contribution weighted by the coefficient α.

By using the numerical procedure presented in Sect. 4.3, we found the evolution of the objective function $h_{1\alpha}$ during the iteration procedure, until the condition of minimum is reached. Let's first consider the structural problem of Fig. 9a, i.e. a rectangular element, assumed to be in plane stress condition, subjected to a simple tensile force.

In Fig. 12 the map of the objective function $h_{1\alpha}$ (for sake of clearness normalized within the range $0 \div 1$), for four different values of the parameter α, is illustrated in the design domain whose boundary values have been assumed as follows: $\nu_{min} \div \nu_{max} = 3.75 \cdot 10^{-5} \div 10^{-3}\ mm/s$, $I_{m,\ min} \div I_{m,max} = 1 \div 450\ W/m^2$. For sake of clarity, the graphical representations provided hereafter are plotted by assuming the normalized value of the design variables, ν', I_m', each of them falling within the range $0 \div 1$, i.e. $\nu'_{min} \div \nu'_{max} = 0 \div 1$ and $I'_{m,\ min} \div I'_{m,max} = 0 \div 1$. Starting from the initial point $\boldsymbol{\xi}_0$, assumed here to be placed at the center of the design domain ($\boldsymbol{\xi}_0 = (\nu', I_m') = (1/2,\ 1/2)$), the final optimal solution – which guarantees the minimum value of $h_{1\alpha}(\nu, I_m)$ – is obtained. The evolution of the optimization problem solution during the iterative procedure is illustrated by the red paths in Fig. 12.

In Fig. 13a the evolution of the objective function $h_{1\alpha}$ is illustrated vs the iteration number, for different values of the weight parameter α; in Fig. 13b the map of the dimensionless shear modulus is reported for the optimal values of the printing variables for the cases $\alpha = 1$ and $\alpha = 10$, while in Fig. 13c the corresponding deformed shapes of the structural elements for $P = 500\ N$ are shown. In Fig. 13c the contour maps display the horizontal displacements, normalized with respect to the displacement of the application point of the force P of the fully cured element, $\bar{\delta}_X^*$. As expected, the objective function involving the highest value of the weight parameter α (=10) provides the less homogeneous material as the asymmetric deformed shape in Fig. 13c confirms.

In Fig. 14a the optimal values of the design variables $\nu,\ I_m$ required to get the minimum condition of the objective function $h_{1\alpha}$ vs the values of the weight parameter α, are displayed, while Fig. 14b illustrates the corresponding minimum values attained by $h_{1\alpha}$, as well as the corresponding value of the dimensionless quantities $\delta', \mathscr{E}'$, involved in the objective function $h_{1\alpha}$, see Eq. (20).

In order to properly set the photopolymerization procedure required to optimize the response of the element in the case of a non-homogeneous stress field, we now consider the same structural element under bending (see Fig. 15a); the mechanical response is here investigated through a nonlinear FE analysis by loading the element up to the value $P = 20\ N$.

In order to emphasize the role by a non-constant absorbance during the solidification, by using the parameters reported at the end of sect. 6 hereafter we consider its variability according to Eq. (7). By assuming $C_I(\boldsymbol{X},\ 0) = 20\ m^3/mol$, from Eq. (7) it can be noticed that when the material is in a liquid state (before curing, i.e. $\varrho(\boldsymbol{X},\ 0) = 0$) we get $A_L = 600\ m^{-1}$, which is the value corresponding to the purely liquid resin used in the previous example where its variation during the curing process was neglected. On the other hand, when the material attains the fully cured condition, the photoinitiator as well as the monomer concentration reduce (i.e. $C_I \to 0$, $C_M \to 0$ while $\varrho \to 1$) and the upper limit of the absorbance $A_U = 2400\ m^{-1}$, corresponding to the fully solid polymer, is attained. Therefore, in a real curing process $A_L \le A(\boldsymbol{x},t) \le A_U$, where A_L and A_U are the lower and upper limits of the absorbance, respectively. By using the

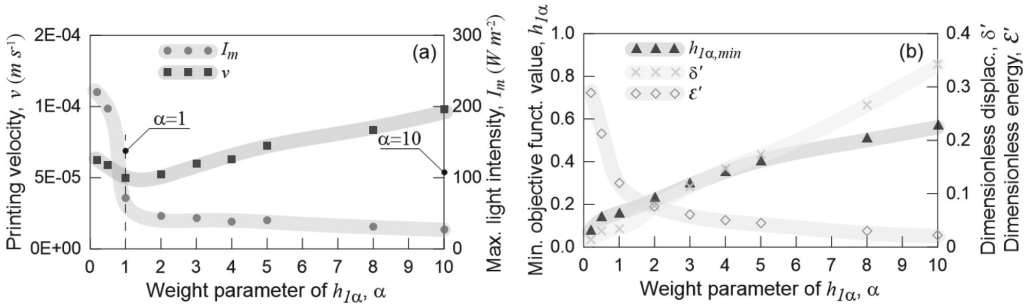

Fig. 14. (Color online) (a) Optimal values of the design parameters v, I_m for different values of the parameter α used to define the objective function $h_{1\alpha}$. (b) Corresponding values of the dimensionless horizontal displacement δ' and energy $\mathscr{E}'$ and of the minimum value attained by the objective function $h_{1\alpha}$.

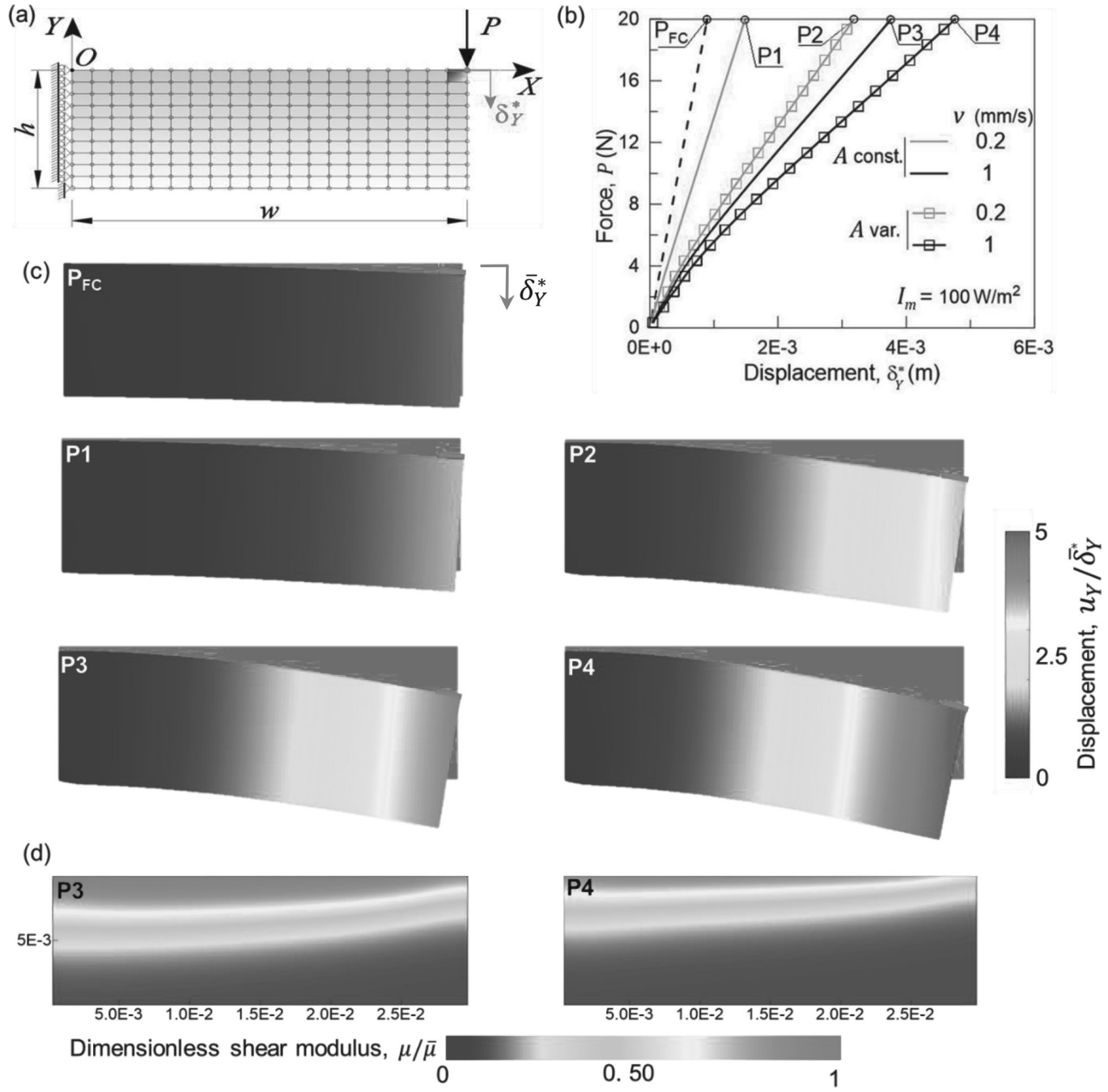

Fig. 15. (Color online) (a) FE discretization of the structural element investigated. (b) Load-displacement curves for two different photopolymerization setups, by assuming both constant and variable material absorbance (P1-P4). (c) Dimensionless vertical displacement field for the fully cured component (P_{FC}) and for the components produced by using the setups (P1-P4). The maps have been plotted by normalizing the vertical displacements with respect to that of the top right point of the fully cured element, $\overline{\delta}_Y^*$. (d) Maps of the dimensionless shear modulus reached at the end of the photopolymerization. Dimensions in [m].

parameters adopted in this example, we have 600 $m^{-1} \leq A(X,t) \leq 2400\ m^{-1}$.

Fig. 15b illustrates the load-displacement curves for the bended element, whose photopolymerization have been simulated by assuming both a constant absorbance $A_L = 600\ m^{-1}$ (the one of the liquid monomer) and that evolving according to Eq. (7), $A(\boldsymbol{X},t)$. For these two cases we simulate the curing process by adopting $v = 2 \cdot 10^{-4}\ m/s$, (P1 and P2 in Fig. 9), and $v = 1 \cdot 10^{-3}\ m/s$ (P3 and P4 in Fig. 9). In each simulation the maximum laser light intensity is assumed to be $I_m = 100\ W/m^2$.

As can be appreciated from Fig. 15b, for a given printing setup the structural element is characterized by a lower stiffness in the case of a variable absorbance with respect to the case with a constant absorbance. The lower stiffness obtained when the absorbance is variable is more pronounced for the lowest laser speed (green curves, P1 and P2, Fig. 15b). On the other hand, such a difference is less evident for the printing setup characterized by the highest laser speed (black curves, P3 and P4, Fig. 15b). This can be explained by considering the evolution equation of the material's absorbance, Eq. (7): a lower laser speed provides an higher degree of cure

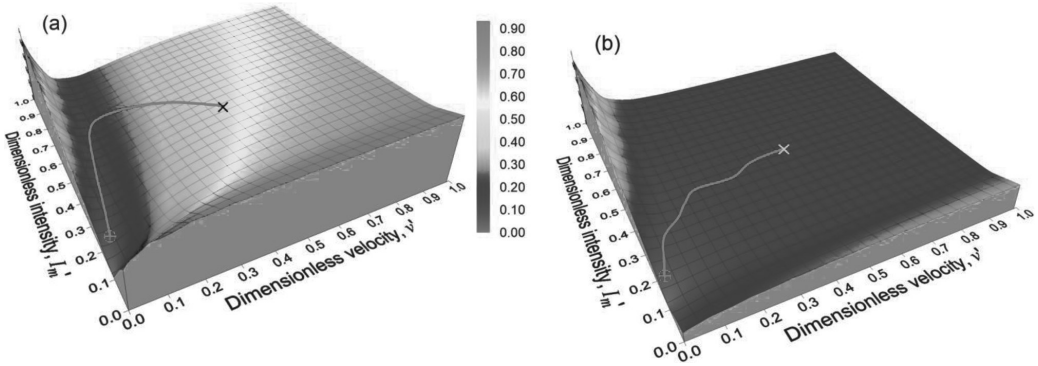

Fig. 16. (Color online) Map of the normalized objective function $h_{1\alpha}$ for the weight parameter $\alpha = 1$ by assuming a constant value of the absorbance (a) and an absorbance variable according to Eq. (7) (b). The solution of the optimization problem evolves as indicated by the red paths, starting from the initial point $\times$ (assumed centered in the design domain) and ending at the optimal point $\oplus$.

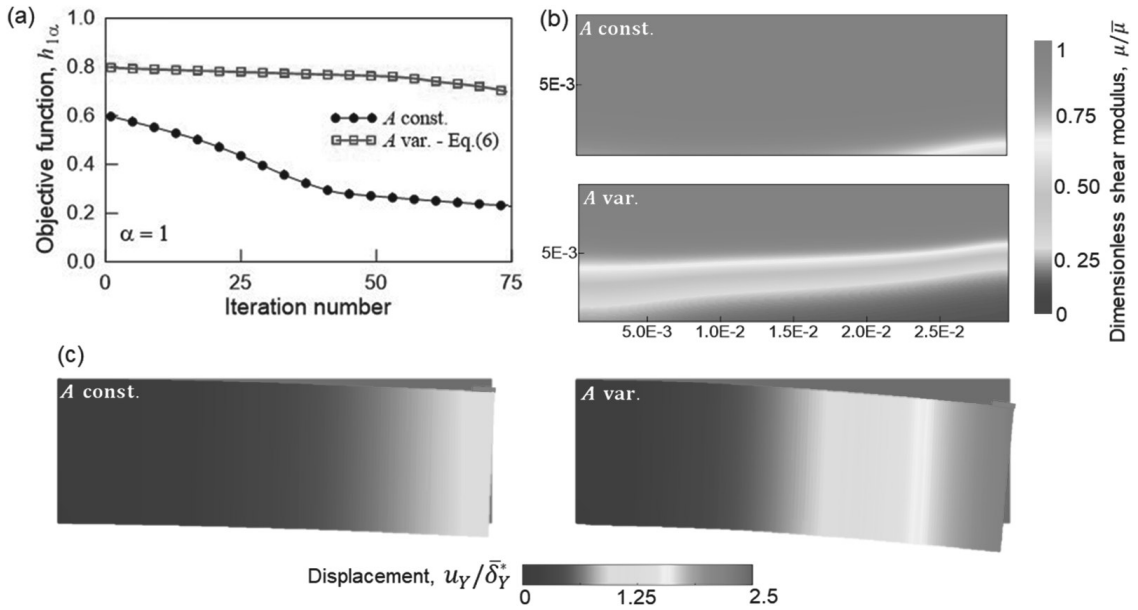

Fig. 17. (Color online) (a) Evolution of the objective function $h_{1\alpha}$ during the optimization iterations by assuming a constant or a variable (according to Eq. (7)) absorbance. (b) Dimensionless shear modulus in the final component obtained by using the best values of the design parameters $v,\ I_m$ evaluated for $\alpha = 1$ when $A = const.$ and $A = var.$ (c) Deformed configurations corresponding to (b) with maps of the dimensionless vertical displacement. Dimensions in [m].

(especially in the top region of the material being printed) where the absorbance heavily increases ($A(\boldsymbol{X},t) > A_L$), thus hindering the curing of the bottom zone of the element; compared to the cases with constant absorbance, this provides a noticeable decreasing of the stiffness. Moreover, the highest laser speed provides a lower degree of conversion, i.e. a lower increase of the absorbance with respect to that of the liquid monomer takes place, leading to a less pronounced decrease of the element's stiffness.

The deformed shapes of the bended element, Fig. 15c, highlight how considerably different can be the mechanical responses by using various photopolymerization setups. Finally, by considering a constant or a variable absorbance for an assumed printing setup, Fig. 15d shows the maps of the dimensionless shear modulus reached at the end of the curing process within the investigated structural element: it clearly demonstrates that a constant material absorbance (that of the liquid monomer) increases the depth of the cured zone (P3, Fig. 15d) in comparison to a DoC-dependent absorbance that shields the photopolymerization (P4, Fig. 15d).

In Fig. 16 the surface plot of the objective function $h_{1\alpha}$ for $\alpha = 1$ (normalized within the range $0 \div 1$), is reported for a constant (Fig. 16a) and a variable (Fig. 16b) absorbance. When A is constant, the objective function $h_{1\alpha}$ presents a narrow region where it reaches a nearly constant minimum value (Fig. 16a), while when A is variable with ϱ such a behavior cannot be clearly observed (Fig. 16b). The evolution of the solution of the optimization problem during the iterative procedure is illustrated by the red paths in Fig. 16; starting from the initial state, assumed to be at the center of the design domain ($\boldsymbol{\xi}_0 = (1/2,\ 1/2)$), the final optimal solution is obtained.

In Fig. 17a the evolution of the objective function $h_{1\alpha}$ evaluated along the optimization iterations corresponding to the paths in Fig. 16, is illustrated; the case with a constant value of the absorbance shows the tendency to reach a minimum, while when A is variable with ϱ such a behavior cannot be clearly observed. The dimensionless shear modulus maps (Fig. 17b) and the deformed configurations (Fig. 17c) corresponding to the two above-mentioned cases are shown in the same figure. It appears clearly that, by considering a gradual variation of the material absorbance, the top part of the material photopolymerizes first and acts as a barrier with respect to the underneath material, leading to a lower chain density in the bottom region of the printed layer. In this way, the achieved optimum condition is significantly different from the fully cured condition, while when the constant absorbance A_L is adopted such a difference is reduced.

The last mechanical optimization problem, related to the objective function $h_{2\beta}(v, I_m)$ (Eq. (21a)), consists in finding the condition of least viscous behavior of the material while using the minimum amount of energy used for printing, the latter quantity weighted by the coefficient β.

In Fig. 18 the contour maps of the objective function $h_{2\beta}$ (normalized within the range $0 \div 1$) for different values of the parameter β, is illustrated in the design domain whose parameters fall within the interval $0 \div 1$. The evolution of the solution during the iteration process, evaluated starting from the initial state, placed at the center of the design domain ($\boldsymbol{\xi}_0 = (1/2,\ 1/2)$) and ending at the site of the minimum of $h_{2\beta}$, is illustrated by the red paths in Fig. 18.

In Fig. 19a the evolution of the objective function $h_{2\beta}$ for different values of the weight parameter β is illustrated vs the iteration number, while in Fig. 19b the map of the dimensionless shear modulus for the optimal values of the printing variables when $\beta = 1$ and $\beta = 10$ is reported.

Finally, Fig. 20a illustrates the optimal values of the design variables $v,\ I_m$ required to obtain the minimum value of the objective function $h_{2\beta}$ vs the values of the weight parameter β, while Fig. 20b provides the corresponding (minimum) values attained by $h_{2\beta}$ and

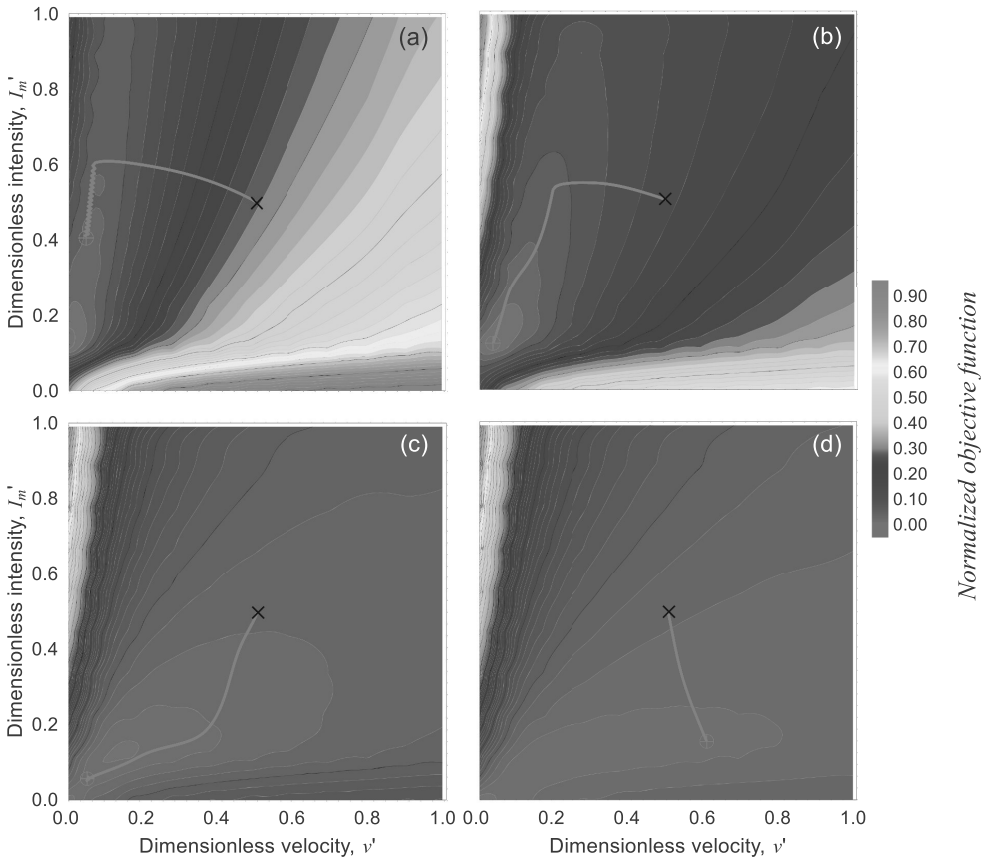

Fig. 18. (Color online) Map of the normalized objective function $h_{2\beta}$ for different values of the parameter β: (a) $\beta = 0.2$, (b) $\beta = 1$, (c) $\beta = 5$ and (d) $\beta = 10$. The solution of the optimization problem evolves as indicated by the red paths, starting from the initial point (assumed centered in the design domain) and ending at the optimal point $\oplus$.

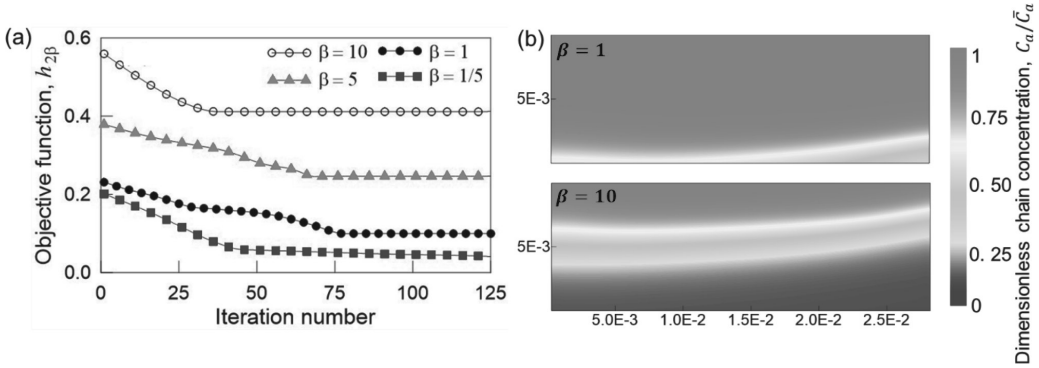

Fig. 19. (Color online) (a) Evolution of the objective function $h_{2\beta}$ during the optimization iterations for different values of the parameter β. (b) Maps of the network chains density within the element's obtained by using the best design parameters ν, I_m estimated by the minimization procedure using $\beta = 1$ and $\beta = 10$. Dimensions in [m].

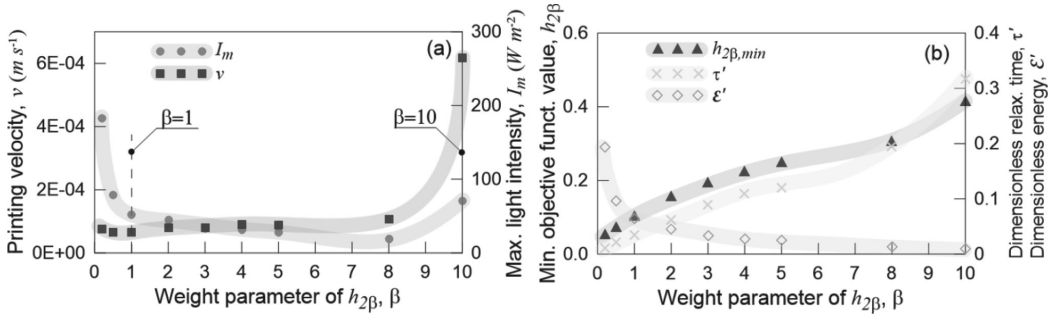

Fig. 20. (Color online) (a) Optimal values of the design parameters v, I_m for different values of the parameter β: (b) Corresponding values of the dimensionless relaxation time and energy required for the photopolerization, τ', $\mathscr{E}'$ and of the minimum value attained by the objective function $h_{2\beta}$.

the dimensionless relaxation time τ' and dimensionless energy spent $\mathscr{E}$.

From the above examples, it emerges that the way the photopolymerization process is performed has a strong effect on the final mechanical properties of the printed element. By properly setting the photopolymerization parameters (i.e. the light intensity and the laser beam velocity), the performance of the element can be heavily increased.

Moreover, accounting for the variability of the absorbance plays a crucial role in determining the final mechanical properties of the printed structural element; we have demonstrated that, by assuming a constant absorbance (that of the liquid monomer) during the whole photopolymerization process, an overestimation of the mechanical properties is obtained, especially for low printing velocities. Analogous considerations can be done for the rate constants involved in the governing chemical kinetics of photopolymerization that, for the sake of simplicity, we have assumed to be constant.

7. Conclusions

In the present paper, a theoretical multiphysics approach describing the photopolymerization process of polymers, typically used in additive manufacturing technologies (often known as stereolithography, SLA), has been presented. This polymer production technique enables us to print objects at a very small scale, making it very attractive for advanced nanotechnological applications.

The light diffusion phenomenon through the medium as well as the polymer chain formation and the mechanics of the resulting material have been mathematically described through a multiphysics micromechanical model. Further, its numerical implementation within a FE framework has been briefly addressed and the problem of the optimum photopolymerization, aimed at minimizing a suitable mechanics-based objective function, has been illustrated. Several numerical examples performed for studying the properties of the photopolymerized material have been presented; in particular, the parametric analyses simulating the solidification process have shown that the adopted approach quantitatively provides the distribution of the chain concentration and the elastic characteristics distribution within the material. The effect of the photopolymerization parameters on the quality of the final polymer have been underlined, and the mechanical behavior of structural elements printed with different photopolymerization setups has been investigated. It has been shown that a wide range of mechanical response arises by slightly varying the photopolymerization parameters. The simulation of the photopolymerization process in a real case has also been illustrated; in particular, the role played by the oxygen inhibition and the material light absorbance during the solidification process has emerged to be fundamental.

The optimization problem, consisting in defining the optimal printing setting required for producing a polymeric element fulfilling some optimal conditions of mechanics-based objective functions, have been finally addressed; we have considered the minimization of the element's compliance and of the printing energy consumption, by adopting the speed of the light source and its intensity as design parameters.

Thanks to its physics-based nature, the proposed approach represents a comprehensive tool to simulate the complex photopolymerization process; it can be used as a tool suitable to control the optimum production or for assessing additively manufactured polymers obtained through the photopolymerization technology. However, the problem of simulating the solidification process of a photopolymerized polymer involves many further aspects to be accounted for, such as the heat flow and the related temperature variation during the process, the role played by secondary chemical agents, etc. Despite its simplicity, the microscale model here proposed captures the main physical and chemical aspects involved and enable us to estimate the distribution of the mechanical properties of a photopolymerized material. A further extension of the proposed approach should consider the solidification layer by layer, as typically done in real AM processes, and the effect of the temperature arising in the material being photopolymerized.

Authors' statement

R.B.: Conceptualization, Methodology, Software, Writing-original draft preparation;
M.P.C.: Methodology, Software, Numerical simulations, Graphical visualization, Final reviewing.

Funding

The authors would like to thank the support from European Union's Horizon 2020 research and innovation program (H2020-WIDESPREAD-2018, SIRAMM) under grant agreement No 857124.

Declaration of Competing Interest

The authors declare that they have no conflicts of interest to report regarding the present study.

References

Anastasio, R., Peerbooms, W., Cardinaels, R., Van Breemen, L.C.A., 2019. Characterization of ultraviolet-cured methacrylate networks: from photopolymerization to ultimate mechanical properties. Macromolecules 52, 9220–9231. https://doi.org/10.1021/acs.macromol.9b01439.

Andrzejewska, E., 2001. Photopolymerization kinetics of multifunctional monomers. Prog. Polym. Sci. 26, 605–665. https://doi.org/10.1016/S0079-6700(01)00004-1.

Andrzejewska, E., Grajek, K., 2017. Recent advances in photo-induced free-radical polymerization. MOJ Polym. Sci. 58–60.

Arruda, E.M., Boyce, M.C., 1993. A three-dimensional constitutive model for the large stretch behavior of rubber elastic materials. J. Mech. Phys. Solids 41 (2), 389–412. https://doi.org/10.1016/0022-5096(93)90013-6.

Bella, F., Bongiovanni, R., 2013. Photoinduced polymerization: an innovative, powerful and environmentally friendly technique for the preparation of polymer electrolytes for dye-sensitized solar cells. J. Photochem. Photobiol. C 16, 1–21. https://doi.org/10.1016/j.jphotochemrev.2013.03.002.
Bikas, H., Stavropoulos, P., Chryssolouris, G., 2016. Additive manufacturing methods and modelling approaches: a critical review. Int. J. Adv. Manuf. Technol. 83, 389–405. https://doi.org/10.1007/s00170-015-7576-2.
Bowman, C.N., Kloxin, C.J., 2008. Toward an enhanced understanding and implementation of photopolymerization reactions. AIChE J. 54, 2775–2795. https://doi.org/10.1002/aic.11678.
Brighenti, R., Cosma, M.P., 2020. Swelling mechanism in smart polymers responsive to mechano-chemical stimuli. J. Mech. Phys. Solids 143, 104011. https://doi.org/10.1016/j.jmps.2020.104011.
Brighenti, R., Cosma, M.P., Marsavina, L., Spagnoli, A., Terzano, M., 2020. Laser-based additively manufactured polymers: a review on processes and mechanical models. J. Mater. Sci. https://doi.org/10.1007/s10853-020-05254-6.
Brighenti, R., Rabczuk, T., Zhuang, X., 2021. Phase field approach for simulating failure of viscoelastic elastomers. Eur. J. Mech. A. Solids 85, 104092. https://doi.org/10.1016/j.euromechsol.2020.104092.
Buss, B.L., Miyake, G.M., 2018. Photoinduced controlled radical polymerizations performed in flow: methods, products, and opportunities. Chem. Mater. 30, 3931–3942. https://doi.org/10.1021/acs.chemmater.8b01359.
Chen, M., Zhong, M., Johnson, J.A., 2016. Light-controlled radical polymerization: mechanisms, methods, and applications. Chem. Rev. 116, 10167–10211. https://doi.org/10.1021/acs.chemrev.5b00671.
Coleman, B.D., Noll, W., 1961. Foundations of linear viscoelasticity. Rev. Mod. Phys. 33, 239–249. https://doi.org/10.1103/RevModPhys.33.239.
Davis, A.B., Marshak, A., 2004. Photon propagation in heterogeneous optical media with spatial correlations: enhanced mean-free-paths and wider-than-exponential free-path distributions. J. Quant. Spectrosc. Radiat. Transfer 84, 3–34. https://doi.org/10.1016/S0022-4073(03)00114-6.
de Gennes, P.G., Leger, L., 1982. Dynamics of entangled polymer chains. Annu. Rev. Phys. Chem. 33, 49–61. https://doi.org/10.1146/annurev.pc.33.100182.000405.
Doi, M., 1996. Introduction to Polymer Physics. Oxford University Press.
Dupaix, R.B., Boyce, M.C., 2007. Constitutive modeling of the finite strain behavior of amorphous polymers in and above the glass transition. Mech. Mater. 39 (1), 39–52. https://doi.org/10.1016/j.mechmat.2006.02.006.
Fleer, G.J., Skvortsov, A.M., 2012. Reconciling lattice and continuum models for polymers at interfaces. J. Chem. Phys. 136 (13), 134707 https://doi.org/10.1063/1.3693515.
Flory, P.J., 1969. Statistical Mechanics of Chain Molecules. Wiley-Interscience, New York.
Flory, P.J., 1953. Principles of Polymer Chemistry. Cornell University Press.
Flory, P.J., Gordon, M., Flory, P.J., McCrum, N..G., 1976. Statistical thermodynamics of random networks. Proc. R. Soc. Lond.. A. Math. Phys. Sci. 351, 351–380. https://doi.org/10.1098/rspa.1976.0146.
Flory, P.J., Rehner, J., 1943. Statistical mechanics of cross-linked polymer networks I. Rubberlike elasticity. J. Chem. Phys. 11, 512–520. https://doi.org/10.1063/1.1723791.
Gordon, M., 1975. The Physics of Rubber Elasticity /by L.R.G. Treloar, 3rd ed. ed. Clarendon Oxford.
Gartner III, T.E., Jayaraman, A., 2019. Modeling and simulations of polymers: a roadmap. Macromolecules 52 (3), 755–786. https://doi.org/10.1021/acs.macromol.8b01836.
Jha, K.C., Tsige, M., 2013. Molecular modeling of thermal and mechanical properties of elastomers: a review. Rubber Chem. Technol. 86 (3), 401–422. https://doi.org/10.5254/rct.13.86985.
Kegl, M., Butinar, B.J., Kegl, B., 2002. An efficient gradient-based optimization algorithm for mechanical systems. Commun. Numer. Methods Eng. 18, 363–371. https://doi.org/10.1002/cnm.499.
Lalitha Sridhar, S., Vernerey, F.J., 2018. The chain distribution tensor: linking nonlinear rheology and chain anisotropy in transient polymers. Polymers (Basel) 10, 848. https://doi.org/10.3390/polym10080848.
Laun, H.M., Bung, R., Schmidt, F., 1991. Rheology of extremely shear thickening polymer dispersionsa) (passively viscosity switching fluids). J. Rheol. 35, 999–1034. https://doi.org/10.1122/1.550257.
Lewandowski, R., Chorążyczewski, B., 2010. Identification of the parameters of the Kelvin–Voigt and the Maxwell fractional models, used to modeling of viscoelastic dampers. Comput. Struct. 88, 1–17. https://doi.org/10.1016/j.compstruc.2009.09.001.
Long, K.N., Scott, T.F., Qi, H.J., Bowman, C.N., Dunn, M.L., 2009. Photomechanics of light-activated polymers. J. Mech. Phys. Solids 57, 1103–1121. https://doi.org/10.1016/j.jmps.2009.03.003.
Long, R., Qi, H.J., Dunn, M.L., 2013. Thermodynamics and mechanics of photochemcially reacting polymers. J. Mech. Phys. Solids 61, 2212–2239. https://doi.org/10.1016/j.jmps.2013.06.008.
Marrucci, G., Bhargava, S., Cooper, S.L., 1993. Models of shear-thickening behaviour in physically crosslinked networks. Macromolecules 26, 6483–6488. https://doi.org/10.1021/ma00076a027.
Nocedal, J., Wright, S., 2006. Numerical Optimization. Springer Science & Business Media.
Perry, M.F., Young, G.W., 2005. A mathematical model for photopolymerization from a stationary laser light source. Macromol. Theory Simul. 14, 26–39. https://doi.org/10.1002/mats.200400056.
Phillips, R., 1984. Photopolymerization. J. Photochem. 25, 79–82. https://doi.org/10.1016/0047-2670(84)85016-9.
Rubinstein, M., Colby, R.H., 2003. Polymer Physics. Oxford University Press.
Sain, T., Loeffel, K., Chester, S., 2018. A thermo–chemo–mechanically coupled constitutive model for curing of glassy polymers. J. Mech. Phys. Solids 116, 267–289. https://doi.org/10.1016/j.jmps.2018.04.001.
Shao, J., Huang, Y., Fan, Q., 2014. Visible light initiating systems for photopolymerization: status, development and challenges. Polym. Chem. 5, 4195–4210. https://doi.org/10.1039/C4PY00072B.
Talebi, H., Silani, M., Bordas, S.P., Kerfriden, P., Rabczuk, T., 2014. A computational library for multiscale modeling of material failure. Comput. Mech. 53 (5), 1047–1071. https://doi.org/10.1007/s00466-013-0948-2.
Treloar, L.R.G., 1946. The elasticity of a network of long-chain molecules.—III. Trans. Faraday Soc. 42, 83–94. https://doi.org/10.1039/TF9464200083.
Valavala, P.K., Clancy, T.C., Odegard, G.M., Gates, T.S., 2007. Nonlinear multiscale modeling of polymer materials. Int. J. Solids Struct. 44 (3–4), 1161–1179. https://doi.org/10.1016/j.ijsolstr.2006.06.011.
Vernerey, F.J., Long, R., Brighenti, R., 2017. A statistically-based continuum theory for polymers with transient networks. J. Mech. Phys. Solids 107, 1–20. https://doi.org/10.1016/j.jmps.2017.05.016.
Vorov, O.K., Livesay, D.R., Jacobs, D.J., 2008. Conformational entropy of an ideal cross-linking polymer chain. Entropy (Basel) 10, 285–308. https://doi.org/10.3390/e10030285.
Williams, M.C., 1975. Molecular rheology of polymer solutions: interpretation and utility. AIChE J. 21, 1–25. https://doi.org/10.1002/aic.690210102.
Vu-Bac, N., Lahmer, T., Zhuang, X., Nguyen-Thoi, T., Rabczuk, T., 2016. A software framework for probabilistic sensitivity analysis for computationally expensive models. Adv. Eng. Software 100, 19–31. https://doi.org/10.1016/j.advengsoft.2016.06.005.
Wu, J., Zhao, Z., Hamel, C.M., Mu, X., Kuang, X., Guo, Z., Qi, H.J., 2018. Evolution of material properties during free radical photopolymerization. J. Mech. Phys. Solids 112, 25–49. https://doi.org/10.1016/j.jmps.2017.11.018.
Xu, D., Hawk, J.L., Loveless, D.M., Jeon, S.L., Craig, S.L., 2010. Mechanism of shear thickening in reversibly cross-linked supramolecular polymer networks. Macromolecules 43, 3556–3565. https://doi.org/10.1021/ma100093b.
Yamaguchi, K., Nakamoto, T., 1998. Micro fabrication by UV laser photopolymerization. Memoirs. Sch. Eng., Nagoya Univ. 50, 33–82.
Zarrelli, M., Skordos, A.A., Partridge, I.K., 2010. Toward a constitutive model for cure-dependent modulus of a high temperature epoxy during the cure. Eur. Polym. J. 46, 1705–1712. https://doi.org/10.1016/j.eurpolymj.2010.06.002.